NUMERICAL INVESTIGATION OF LIVING CELLS UNDER ULTRASONIC EXCITATION IN MICROFLUIDIC DEVICES

A THESIS SUBMITTED TO
THE GRADUATE SCHOOL OF NATURAL AND APPLIED SCIENCES
OF
MIDDLE EAST TECHNICAL UNIVERSITY

BY

HANDE NUR AÇIKGÖZ

IN PARTIAL FULFILLMENT OF THE REQUIREMENTS
FOR
THE DEGREE OF MASTER OF SCIENCE
IN
MECHANICAL ENGINEERING

DECEMBER 2020

Approval of the thesis:

NUMERICAL INVESTIGATION OF LIVING CELLS UNDER ULTRASONIC EXCITATION IN MICROFLUIDIC DEVICES

submitted by **HANDE NUR AÇIKGÖZ** in partial fulfillment of the requirements for the degree of **Master of Science in Mechanical Engineering, Middle East Technical University** by,

Prof. Dr. Halil Kalıpçılar
Dean, Graduate School of **Natural and Applied Sciences** ________________

Prof. Dr. Mehmet Ali Sahir Arıkan
Head of the Department, **Mechanical Engineering** ________________

Assoc. Prof. Dr. Mehmet Bülent Özer
Supervisor, **Mechanical Engineering, METU** ________________

Examining Committee Members:

Assoc. Prof. Dr. Yiğit Yazıcıoğlu
Mechanical Engineering, METU ________________

Assoc. Prof. Dr. Mehmet Bülent Özer
Mechanical Engineering, METU ________________

Assoc. Prof. Dr. Ender Yıldırım
Mechanical Engineering, METU ________________

Prof. Dr. Selin Aradağ Çelebioğlu
Mechanical Engineering., TED University ________________

Assoc. Prof. Dr. Barbaros Çetin
Mechanical Engineering, Bilkent University ________________

Date: 28.12.2020

I hereby declare that all information in this document has been obtained and presented in accordance with academic rules and ethical conduct. I also declare that, as required by these rules and conduct, I have fully cited and referenced all material and results that are not original to this work.

Name, Last name : Hande Nur Açıkgöz

Signature :

ABSTRACT

NUMERICAL INVESTIGATION OF LIVING CELLS UNDER ULTRASONIC EXCITATION IN MICROFLUIDIC DEVICES

Açıkgöz, Hande Nur
Master of Science, Mechanical Engineering
Supervisor : Assoc. Prof. Dr. Mehmet Bülent Özer

December 2020, 84 pages

Acoustophoretic microfluidic applications are an essential part of Lab-on-a-chip systems. Studies about acoustophoretic particle manipulation are available in the literature. However, conventional analytical methods fall short of including many factors affecting acoustophoretic manipulation of biological samples when applied to biological systems. Therefore, numerical methods become useful tools to investigate the phenomena to a larger extent. This thesis aims to analyze the factors of particle geometry, sample concentration, and the channel wall effect. To go beyond the isolated particle assumption, methods presented take the particle's acoustic interaction with other particles and channel walls into consideration while putting no restriction on particle shape. The acoustic simulation model, created for this purpose, is integrated into a code for hydrodynamic calculations to obtain particle trajectories under different circumstances. The coupled method renders acoustophoretic particle manipulation simulations in microfluidic channels and includes both acoustic and hydrodynamic interactions.

Keywords: Acoustic Radiation Force, Numerical Simulations, Cell

ÖZ

CANLI HÜCRELERİN MİKROAKIŞKAN CİHAZLARDAKİ AKUSTİK UYARIMININ NÜMERİK OLARAK İNCELENMESİ

Açıkgöz, Hande Nur
Yüksek Lisans, Makina Mühendisliği
Tez Yöneticisi: Doç. Dr. Mehmet Bülent Özer

Aralık 2020, 84 sayfa

Akustoforetik mikroakışkan uygulamaları, Çip-Üstü-Laoratuvar sistemlerinin önemli bir parçasıdır. Literatürde akustoforetik parçacık manipülasyonu ile ilgili çalışmalar mevcuttur. Bununla birlikte, bilinen analitik yöntemler, biyolojik sistemlere uygulandığında biyolojik numunelerin akustoforetik manipülasyonunu etkileyen birçok faktörü dahil etmekte yetersiz kalmaktadır. Bu nedenle, sayısal yöntemler, bu fenomeni daha büyük ölçüde araştırmak için yararlı araçlar haline gelmektedir. Bu tez, parçacık geometrisi, numune konsantrasyonu ve kanal duvarı etkisi gibi faktörleri incelemeyi amaçlamaktadır. Sunulan yöntemler, izole parçacık varsayımının ötesine geçmek için, diğer parçacıklarla ve kanal duvarlarıyla akustik etkileşimi dikkate alır ve aynı zamanda parçacık şekli üzerinde herhangi bir sınırlama getirmez. Bu amaçla oluşturulan akustik simülasyon modeli, farklı koşullar altında parçacık yörüngelerini elde etmek için, bir hidrodinamik hesaplama koduna entegre edilmiştir. Birleştirilmiş yöntem, mikroakışkan kanallarda akustoforetik parçacık manipülasyonu simülasyonlarını gerçekleştirir ve hem akustik hem de hidrodinamik etkileşimleri içerir.

Anahtar Kelimeler: Akustik Radyasyon Kuvveti, Sayısal Yöntemler, Hücre

ACKNOWLEDGMENTS

The author wishes to express her deepest gratitude for the contributions to this thesis and the support:

- My supervisor Assoc. Prof. Dr. Mehmet Bülent Özer for his guidance, advice, criticism, encouragement, and insight throughout the research.
- Assoc. Prof. Dr. Barbaros Çetin for his suggestions and comments and sharing the code for hydrodynamic calculations used extensively in this thesis, and Atakan Atay for his help in implementing the code.
- All my friends for motivating me and for the good time we had together.

Finally, I would like to thank my family for always believing in me and supporting me my whole life.

TABLE OF CONTENTS

LIST OF TABLES

TABLES

LIST OF FIGURES

FIGURES

LIST OF ABBREVIATIONS

ABBREVIATIONS

BEM	Boundary Element Method
FEM	Finite Element Method
RBC	Red Blood Cell
1D	One dimensional
2D	Two dimensional
3D	Three dimensional

LIST OF SYMBOLS

SYMBOLS

a	[m/s^2]	Acceleration
α	[m]	Particle radius
c_0	[m/s]	Speed of sound in fluid
c_p	[m/s]	Speed of sound in particle
C	[Ns/m]	General drag coefficient
C_v	-	Shape coefficient for drag force
d	[m]	Distance
D	[m]	Particle diameter
E_{ac}	[J/m^3]	Acoustic Energy Density
ε	-	Spheroid shape parameter
f	[Hz]	Acustic wave frequency
f_1	-	Coefficient for density
f_2	-	Coefficient for compressibility
$\overrightarrow{F_d}$	[N]	Hydrodynamic drag force
$\overrightarrow{F_r}$	[N]	Acoustic radiation force
$\overrightarrow{F_{r2}}$	[N/m]	Acoustic radiation force in 2D
k	[1/m]	Wave number
L	[m]	Channel width
L_H	[Ns/m]	Drag coefficient matrix
$\vec{n}$	-	Surface normal vector
p	[Pa]	Pressure field
p_{in}	[Pa]	Incident pressure field
P_0	[Pa]	Pressure amplitude
p_0	[Pa]	Zero order pressure field
p_1	[Pa]	First order pressure field

p_2	[Pa]	Second order pressure field
$\vec{r}$	[m]	Position vector
$\vec{r}_p$	[m]	S
Re	-	Reynolds number
S	[m^2]	Particle surface
S_0	[m^2]	Fixed particle surface
t	[s]	Time
T_r	[Nm]	Acoustic radiation torque
T_{r2}	[N]	Acoustic radiation torque in 2D
$\vec{u}$	[m/s]	Particle velocityvector
u_1	[m/s]	Particle velocity in x-axis
u_2	[m/s]	Particle velocity in y- axis
u_3	[m/s]	Particle velocity in z- axis
$\overrightarrow{U_r}$	[J]	Gork'kov potential
ω	[rad/s]	Angular velocity around z-axis
ω_f	[rad/s]	Angular frequency
$\vec{v}$	[m/s]	Velocity vector field
$\overrightarrow{v_1}$	[m/s]	First order velocity vector field
$\overrightarrow{v_2}$	[m/s]	Second order velocity vector field
$\overrightarrow{v_{in}}$	[m/s]	Incident velocity vector field
x,y,z	[m]	Spatial coordinates
γ	-	Euler's constant
λ	[m]	Acoustic wavelength
μ	[Pa.s]	Dynamic viscosity
ρ	[kg/m^3]	Density
ρ_0	[kg/m^3]	Static fluid density
ρ_1	[kg/m^3]	First order density
ρ_2	[kg/m^3]	Second order density
ρ_p	[kg/m^3]	Particle density

φ	-	Acoustophoretic contrast factor
ψ	[m^2/s]	Acoustic velocity potential
$\emptyset$	[m^2/s]	Acoustic velocity potential independent of time
Ω	[m^3]	Domain where the solution is sought
$\partial\Omega$	[m^2]	Boundary
v_x^i, v_y^i	[m/s]	x and y velocities of particle *i*
w^i	[rad/s]	Angular velocity of particle *i*
x_0^i, y_0^i	[m]	x and y coordinate of particle *i*
F_x^i, F_y^i	[N/m]	Acoustic forces in x and y directions on particle *i*
T^i	[N]	Acoustic torque in z direction on particle *i*
σ_x, σ_y	[N/m^2]	Total stress x and y components

CHAPTER 1

INTRODUCTION

1.1 Acoustophoresis

Acoustophoresis is a phenomenon of the migration of particles in an acoustic field resulting from acoustic waves' scattering from particle surface [1]. The term covers all impacts on particles in a fluid resulting from an acoustic field. Particles suspended within a fluid in an acoustic field tend to move towards the acoustic pressure nodes or antinodes due to the acoustic radiation force exerted on them. This phenomenon is a useful tool for many microfluidic applications. It offers the possibility of spatial control of particles in a fluid by utilizing acoustic waves.

Spatial manipulation of particles can lead to concentration and separation applications. A concentration study aims to increase the particle concentration of the suspension by focusing particles in a smaller area of the channel, while a separation study is used to sort out particles with different size or acoustic properties inside the same suspension. A practical scheme for separation consists of a trifurcated microfluidic channel in which suspension flows continuously. Channel usually has three inlets and three outlets where particle suspension enters the channel from side inlets, and the buffer solution enters from the main inlet. Without any interference, particles will pass through the channel and leave from the side outlets. By applying an acoustic field inside the microfluidic channel, acoustic force will exert on each particle depending on its size and acoustic properties. In an experimental setup, acoustic actuation appears as a standing acoustic wave in channel-width direction and is provided by a piezo-ceramic attached to the microfluidic chip. Considering an acoustic half wave, a pressure nodal line will be generated in the channel centerline. Particles with a greater acoustophoretic force on them will move towards the centerline, while particles experiencing a small force will not. Therefore, these two groups of particles will leave the channel from different outlets. An example of acoustophoretic particle separation study for large, medium and small particles can be seen in Figure 1-1 below.

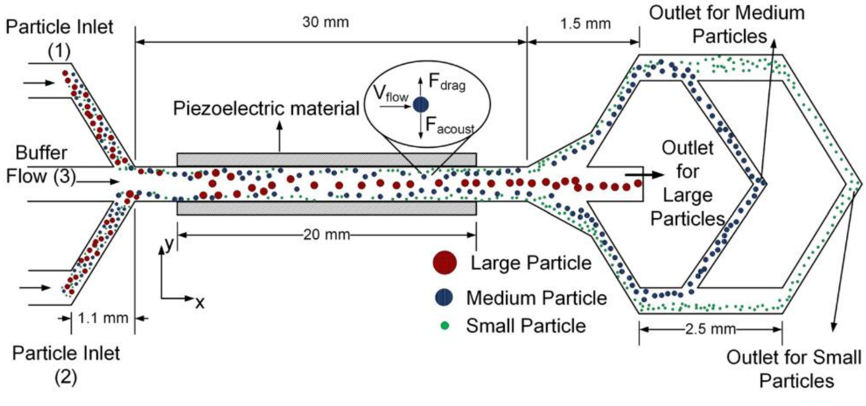

Figure 1-1 Acoustophoretic particle seperation setup [2]

Acoustophoretic manipulation is a suitable tool for biological applications. Concentration/separation of living cells and bacteria for diagnosis and other medical purposes requires cell viability. Compared to other manipulation techniques like filtration, acoustophoresis comes forward as a contactless method that benefits cell viability. Acoustic field does not have a harmful effect on cells, unlike electric and magnetic fields used for dielectrophoresis and magnetophoresis. Apart from these, this method is also cost-efficient. Device fabrication is not complicated or expensive. A wide-range of chip materials can be used.

1.2 Literature Survey

The observed physical phenomenon was first analyzed by King in 1934 [3] for incompressible spheres suspended in an inviscid fluid and later extended to compressible spheres by Yosioka and Kawasima [4]. Gorkov introduced a potential-based approach to calculate acoustic radiation force on particles [5]. The method proposed by Gorkov was summarizing and easy to implement; therefore, it has been used widely in many studies. Later, thermal and viscous effects were also included by Settnes and Bruus [6].

As a label-free and contactless method for particle manipulation, acoustophoresis is a suitable tool for biological applications. Several experimental studies use acoustophoresis for processing biological samples such as enrichment of cancer cells [7], [8], separation of blood cells [9], [10] and bacteria [11], [12], measuring compressibility of cells [13], [14] and determination of hematocrit level [15]. As the given studies show, acoustophoresis can be a useful tool for the manipulation of biological cells. Therefore it has been getting more attention in the last two decades.

There are several simulation studies in the literature that model motion of microparticles in an acoustic field. Most of these studies calculate the acoustic radiation force by well-known Gorkov potential based analytical formulation and using this formulation, they investigate different aspects of acoustophoresis phenomena in microfluidic applications. Muller et al. simulated the acoustophoretic motion of particles suspended in a static fluid medium while accounting for the thermoviscous effects [16]. Gao et al. developed a model for particle focusing patterns in microchannels with nearly square cross-sections while accounting for 2D wave transmission in solid and fluid domains [17]. Yang et al. investigated the effect of several factors, including channel geometry and particle release positions[18]. Liu et al. included the impact of spatial temperature distribution on particle motion in addition to a moving fluid medium, using quadratic mapping functions and finite difference method[19]. Lei et al. modeled a two-stage acoustic separation chip driven by surface acoustic waves with moving fluid medium in 2D [20]. Also, 3D device level FEM simulations of ultrasonic cell separation processes exist. In the study published in 2014 [2], particle separation process is simulated considering the effects of diffusion, particle distribution, and flow rates. Recently, Şahin et al. [21] accounted for chip elastodynamic response of the solid parts.

For the aspect of shape, some studies investigated the motion of non-spherical particles in the acoustic field. Schwarz et al. [22] stated that a non-spherical particle's equilibrium position in an acoustic field can be determined from the force potential derived by Gorkov. They obtained continuous rotation of glass fibers by applying time-varying acoustic field. In their later study [23], Schwarz et al. calculated the acoustic radiation torque on a single elastic fiber by solving the surface integral using FEM. Yamahira et al. studied the rotational control of fibers in a composite material matrix using ultrasound [24]. They assumed the fiber as a chain of spheres and used the formulation of Yosioka and Kawasima [4] to estimate the acoustic forces and torques on fibers. In another study [25], the authors simulated the motion of a microfiber, a microdisk and motion of an RBC in 3D-space using a FEM model while particles are isolated in each case.

Concentration is another concern that has been covered by some studies in the literature. In his study in 2001, Doinikov approached acoustic particle-particle interactions analytically [26]. His model applies for multiple re-scattering events from multiple particles; however, the proposed method is rather too complicated and challenging to implement. Another analytical model of acoustic particle-particle interactions was proposed by Lopes et al. [27]. Yet, this method is valid for the far-field approach and difficult to implement similar to the previous one. Silva and Bruus developed a technique to estimate acoustic interparticle forces analytically from interaction potential energy. Although, it is valid for spherical particles in Rayleigh limit [28]. Rayleigh limit simply refers to a sytem where the particle size is much smaller than the acoustic wavelength. Ley and Bruus [29] performed a different approach to present the concentration effect. In this study, authors used a method called continuum effective medium where the effect of concentration is not simulated with individual particles but rather through the calculation of the impact of concentration on the flow and acoustic force characteristics. Hasegawa investigated the acoustic radiation force on a single particle in an acoustic field theoretically [30]. His solution brings no restriction to particle size, therefore can be applied to the cases beyond Rayleigh limit while it is valid for single particle and it takes no account of the secondary acoustic radiation forces.

Above mentioned studies tried to extend the generic standards in different aspects, which were either about shape, concentration, or frequency (Rayleigh limit). On the other hand, some studies combined different effects to model acoustofluidic phenomena with more accuracy. Glynne-Jones et al. used finite element analysis to calculate acoustic radiation force on a single arbitrarily shaped particle regardless of the Rayleigh limit [31]. In their work in 2017, Baasch et al. [32] calculated multiple spherical particles' trajectories while handling the acoustic particle-particle interactions with an analytical approach and assumes particles to be in Rayleigh limit. Apart from contact forces between particles, hydrodynamic particle-particle interaction is considered which uses a method assuming particles are in an infinite domain. In a later study of Baasch and Dual [33], authors introduce a method that can be used for particles with any shape without any restriction of Rayleigh limit. They simulated the trajectories of multiple spherical particles in 2D acoustic field icluding acoustic and hydrodynamic particle-particle and also introduced contact preventing forces on the particles in the numerical simulation.

1.3 Assumptions and Limitations

Closed-form analytical formulations of acoustic radiation force proposed by many authors are discussed in the previous section. Integration of acoustic pressure over the particle boundary becomes difficult to implement analytically for many cases. In order to evaluate that, some assumptions have to be made. In terms of shape, many analytical studies assumed particle as a sphere, which makes the calculation easier. Therefore, existing solutions in the literature are rather limited to the spherical shape or simple cylindrical shape, Marston's formula [34] is also valid for spheroids with small deviations from the spherical shape.

The second assumption requires that particle size is much smaller than the acoustic wavelength ($\alpha \ll \lambda$), therefore in Rayleigh limit. This limits the analytical solutions to either small particles or low frequencies. Lastly, particle is assumed to be isolated. Thus re-scattering effects due to other existing particles or walls are neglected since the scattering potential is represented by monopole and dipole terms only.

For the hydrodynamic part, a set of assumptions is also prominent. The analytical formulation of Stokes is also based on some assumptions. This approach assumes that particles are spherical and not close to the channel walls. In addition to these, it is assumed that particles or cells' existence does not alter the flow field. Lamb [35] made an extension to the shape with his formulation for a unit length cylinder; however, the isolated particle assumption remained.

Even though these analytical methods were used in many studies in the literature, such an approach may give some inaccurate results due to the following properties of biological systems: Firstly, cells and microorganisms are not always spherical, such as red blood cells in blood and several different classes of bacteria which are not spherical i.e. E. Coli or Helicobacter pylori. Secondly, biological systems may have high concentration of cells such that cells may affect each other both acoustically and hydrodynamically. Blood is a good example of this, since it is a high concentration mixture of cells. Only red blood cells constitute around 40% of the blood volume. Lastly, the acoustic wavelength may not always be large compared to the cells or microorganisms' size. Therefore, Rayleigh limit would not be valid anymore. Sometimes higher frequency in acoustophoresis may be needed to have improved sensitivity. Studies with surface acoustic waves use high-frequency acoustic waves that may be comparable to the size of the biological particle. Therefore, the defined approach above may give low-accuracy results for some biological systems.

1.4 Objective

As stated in the section 1.3, existing analytical solutions for acoustic radiation force and hydrodynamic drag force fail to represent the acoustic manipulation of biological samples in many ways. Several living cells as well as bacteria comes in different shapes and in high concentrations. Without inclusion of the shape and concentration aspects (particle-particle interactions), biological sample manipulations will not be represented completely. On the other hand, analytical scheme for acoustic manipulation of these particles is limited to the small particle assumption. For the applications that require more precise manipulation with higher acoustic frequencies, analytical solutions fail to provide a representation. Assumptions, and limitations brought by them leads the studies to numerical methods. Although the numerical studies investigating these aspects exist in the literature, they are either focused on one of aspects or the combination of some of them.

There are also several issues in terms of computational difficulties due to possible high concentration of particles through meshing in numerical studies. The existence of high number of particles that are very close to each other requires a high-density mesh which causes computation time problems. Also, when the microparticles get very close to each other then it is possible to get mesh errors due to very small meshes required in between the particles which may result in errors and inaccuracies due to decreased mesh quality. Using boundary element method eliminates the need to mesh channel region in between the particles, however BEM is very rarely used in acoustophoretic studies. To the best of found knowledge, there are a few studies which used BEM in acoustophoretic force calculation. However most of them investigate only single cell in the simulations without fluid flow or trajectory of the particle [36]. On the other hand, there are also some studies that include acoustic interactions of a pair of particles using BEM [37], [38], yet they are not focused on particle separation.

In this thesis, it is aimed to develop a numerical tool for the analysis of biological samples in acoustofluidic setups without any limitation regarding particle shape, size or concentration. Therefore it is applicable to non-spherical particles, high concentration samples and to the cases beyond Rayleigh limit. This tool consists of acoustic and hydrodynamic parts. Particle-particle and particle-wall interactions can be handled both in the acoustic part of the simulations as well as the fluid flow part of the simulations without the need for any assumptions about particles being in an infinite domain or having spherical shapes. Boundary element method is used for both acoustic and hydrodynamic parts of the numerical tool which eliminates the need for a high density mesh inside the channel. Also, the proposed simulation method can be used beyond Rayleigh limit. A detailed search on literatue yielded no study in acoustophoresis which does not have the restrictions defined in this paragraph. To the best of my knowledge, this is the first study which uses BEM in both acoustic and fluid domains. Also, in this proposed study FEM can also be used for acoustic or fluidic domain and if needed it can be coupled with BEM solutions of different domains. Although there are a few shape-based separation studies by means of inertial microfluidics [39] and viscoelastic non-Newtonian fluids [40], however, it is the first study which simulates the acoutophoretic separation of non-spherical particles in acoustophoretic device level simulation i.e. including the effects of chip material, piezoelectric actuation and fluid flow inside the channel.

1.5 Outline of the Thesis

This thesis consists of numerical studies designed and used to simulate the acoustophoretic setups in terms of particle movements inside the acoustic microfluidic channel or chambers. Chapter 1 gives an introduction to acoustophoresis and its applications on biological systems. A literature survey is presented, limitations of analytical framework is explained and the objective of the thesis is stated. Chapter 2 gives a brief information about the analytical framework in terms of both acoustic and hydrodynamic forces in the process. Formulations for acoustic radiation force and hydrodynamic drag force are presented. Chapter 3 consists of validation studies of the numerical implementations against analytical methods for designed cases. For the acoustics part, numerically evaluated acoustic radiation force on isolated particles is compared to the analytical results to verify the numerical methods used in this thesis. Numerical FEM based method for hydrodynamic calculations is also verified against analytical formulations. In Chapter 4, several factors discarded by conventional analytical techniques yet effect the acoustic radiation force are investigated. Conditions that create secondary effects on particle manipulation are simulated in a closed cavity using the proposed hybrid MATLAB-COMSOL algorithms. In Chapter 5, 2-dimensional simulations of spherical and non-spherical particles in an acoustofluidic device is presented with the existence of bulk fluid flow.

CHAPTER 2

ACOUSTOPHORESIS THEORY

2.1 Acoustic Radiation Force

Acoustophoresis, meaning migration with sound [41], is a phenomenon that occurs when an ultrasonic acoustic pressure field is applied to a fluid containing particles. Fluid, incited by the acoustic wave, has oscillations in density and velocity, leading to the pressure gradient in the fluid domain. A particle of finite size suspended in the fluid domain will also be exposed to a pressure gradient on it. In the case of a harmonic pressure wave, a harmonic force is exerted on the suspended particle. However, the force value goes to zero when time-averaged. Therefore, to explain the phenomena, non-linear terms of Navier-Stokes equations and the non-zero compressibility of fluid should be included by second-order expansion. Density, pressure and velocity fields $\rho, p, \vec{v}$ are defined as the sum of steady-state terms, linear harmonic terms, and second-order terms.

$$\begin{aligned} \rho &= \rho_0 + \rho_1 + \rho_2 \\ p &= p_0 + p_1 + p_2 \\ \vec{v} &= \vec{0} + \overrightarrow{v_1} + \overrightarrow{v_2} \end{aligned} \tag{1}$$

As Bruus showed that, time-averaged second-order acoustic pressure could be expressed in terms of first-order pressure and velocity fields, assuming inviscid fluid [6]

$$p_2 = \frac{1}{2\rho_0 c_0^2}\langle p_1^2 \rangle - \frac{1}{2}\rho_0 \langle v_1^2 \rangle \tag{2}$$

where ρ_0 and c_0 denote the steady-state density and speed of sound of the fluid. Knowing that, acoustic radiation force acting on an object in an acoustic field is obtained by integrating total acoustic pressure on the particle surface. Considering that the first-order terms are harmonic, their time-averaged value goes zero, leaving only second-order terms. Therefore acoustic radiation force on a fixed particle is found by integrating time-averaged acoustic radiation force over the fixed particle boundary S. For the moving particle, integration should be evaluated over moving particle surface S(t) as given in (3) where $\vec{n}$ is the surface normal vector. To avoid computational difficulties, this integration can be evaluated on fixed particle surface or any surface encompassing the particle by adding a momentum flux term $\rho_0\langle(\vec{n}\cdot\overrightarrow{v_1})\overrightarrow{v_1}\rangle$ as Yosioka and Kawasima stated (4) [4]

$$\overrightarrow{F_r} = -\int_{S(t)} \left\{\left[\frac{1}{2\rho_0 c_a^2}\langle p_1^2\rangle - \frac{1}{2}\rho_0\langle v_1^2\rangle\right]\vec{n}\right\} dS \tag{3}$$

$$\overrightarrow{F_r} = -\int_{S} \left\{\left[\frac{1}{2\rho_0 c_a^2}\langle p_1^2\rangle - \frac{1}{2}\rho_0\langle v_1^2\rangle\right]\vec{n} + \rho_0\langle(\vec{n}\cdot\overrightarrow{v_1})\overrightarrow{v_1}\rangle\right\} dS \tag{4}$$

Similarly, acoustic radiation torque on the particle can be expressed as

$$\overrightarrow{T_r} = -\int_{S} \vec{r}\times\left(\left\{\left[\frac{1}{2\rho_0 c_a^2}\langle p_1^2\rangle - \frac{1}{2}\rho_0\langle v_1^2\rangle\right]\vec{n} + \rho_0\langle(\vec{n}\cdot\overrightarrow{v_1})\overrightarrow{v_1}\rangle\right\} dS\right) \tag{5}$$

where $\vec{r}$ is the position vector directed towards any point on the particle surface. These formulations given above apply for an arbitrarily-shaped particle in an arbitrary acoustic field and give the total acoustic radiation force on the object. However, they are difficult to implement analytically for many geometries.

Closed-form analytical solutions for acoustic radiation force exist in the literature for limited cases. King [3], being the first among others, provided a solution for rigid spheres in standing and traveling acoustic waves. He used infinite series to obtain force on small rigid spheres with sizes much smaller than the acoustic wavelength. His formula for a small rigid sphere in standing acoustic wave is given by

$$F_x = \pi\rho_0|\Phi|^2(ka)^3\sin(2kx)\left(\frac{1+\frac{2}{3}\left(1-\frac{\rho_0}{\rho_1}\right)}{2+\frac{\rho_0}{\rho_1}}\right) \tag{6}$$

where Φ is the velocity potential of the incident wave, $k = \frac{\omega}{c_0}$ is the wavenumber, a is the particle radius, ρ_0 and ρ_1 are the densities of the surrounding fluid and the particle. x is the distance from the pressure antinode in the wave direction. The last parenthesis on the right-hand side of the formula indicates the effect of the particle's properties and the surrounding fluid materials. Later, Yosioka and Kawasima [4] extended the formulation to include the particle's acoustic domain by accounting for the particle as a compressible domain. Their solution for a compressible sphere in standing wave is

$$F_x = \pi\rho_0|\Phi|^2(ka)^3\sin(2kx)\left(\frac{1+\frac{2}{3}\left(1-\frac{\rho_0}{\rho_1}\right)}{2+\frac{\rho_0}{\rho_1}} - \frac{1}{3}\frac{\rho_0 c_0^2}{\rho_1 c_1^2}\right) \tag{7}$$

where c_0 and c_1 refers to the speed of sound values in the surrounding fluid and the particle domains. In 1962, Gorkov [5] proposed a different approach to obtain acoustic radiation force by introducing acoustic force potential whose gradient gives the acoustic force value. Gorkov's formulation for a small elastic sphere placed in an arbitrary acoustic field is as follows

$$U_r = \frac{4\pi}{3}a^3\left[f_1\frac{1}{2\rho_0 c_a^2}\langle p_{in}^2\rangle - f_2\frac{3}{4}\rho_0\langle v_{in}^2\rangle\right]$$

$$\vec{F_r} = -\vec{\nabla}U_r \tag{8}$$

$$f_1 = 1 - \frac{\rho_0 c_0^2}{\rho_1 c_1^2}, \qquad f_2 = \frac{2(\rho_1 - \rho_0)}{2\rho_1 + \rho_0}$$

where f_1 and f_2 are the coefficients depending on material properties. Similar to the general form of the acoustic force (4), Gorkov stated the potential in terms of second order incident pressure field, then evaluated the scattering from a spherical surface by monopole and dipole terms. His formula for standing plane wave takes the form of (9) where E_{ac} is the acoustic energy density in the standing wave, and φ is the acoustic contrast factor equivalent to the term in Yosioka and Kawasima's formulation.

$$F_x = 4\pi E_{ac}(ka)^3\, \varphi \sin(2kx) \quad (9)$$

$$E_{ac} = \frac{P_0^2}{4\rho_0 c_0^2}\,, \qquad \varphi = \frac{\rho_1 + \frac{2}{3}(\rho_1 - \rho_0)}{2\rho_1 + \rho_0} - \frac{1}{3}\frac{\rho_0 c_0^2}{\rho_1 c_1^2}$$

Going beyond the spherical shape limitation, Marston et al. [34] proposed a solution based on the calculation of scattering coefficients for rigid cylinders and rigid spheroids whose symmetry axis is on the wave direction. After that, he implemented his coefficients to Hasegawa's formula to calculate force. Marston' formula for rigid spheroids is given by

$$F_r(\varepsilon) \approxeq F_r(0)\left(1 + \frac{6}{25}\varepsilon + \frac{9}{875}\varepsilon^2 + \cdots\right) \quad (10)$$

$$\varepsilon = \frac{b}{a} - 1$$

where a and b are the radii along the symmetry axis and perpendicular to the symmetry axis, respectively. $F_r(0)$ denotes the force on an equivalent rigid sphere with $\varepsilon = 0$, and is identical to the King's formula for rigid spheres. This formula is known to be valid for $|\varepsilon| \ll 1$.

2.2 Hydrodynamic Drag Force

Stoke's equation [42] in the most basic form (11) expresses the equation for a particle moving inside of a fluid. This equation gives the hydrodynamic viscous drag force exerts on a particle of radius a, moving with a constant velocity of $\vec{u}$ with respect to the fluid with dynamic viscosity of μ. The fluid is viscous, incompressible, and not bounded. It is valid for Stokes flow conditions at low Reynolds numbers ($Re \ll 0.1$) in which inertial effects are neglected.

$$\overrightarrow{F_d} = -6\pi\mu\vec{u}a \quad (11)$$

Analytical derivations for the drag force on spheroids in a steady Stokes flow also exist in the literature. Drag force on a prolate spheroid with eccentricity b/a moving along its axis of symmetry was given by Lai and Mockros [43](12). C_v is the viscous shape coefficient for Stoke's steady-state drag and b is the radius perpendicular to the spheroid's symmetry axis. C_v coefficient depends on the ratio of major and minor axes of the spheroid.

$$\overrightarrow{F_d} = -C_v 6\pi\mu\vec{u}a \tag{12}$$

Drag force exerted on a cylinder of unit length in a Stokes flow with low Reynolds number was formulated by Lamb as follows [35]:

$$\overrightarrow{F_d} = -\frac{4\pi\mu\vec{u}}{\frac{1}{2}-\gamma-\ln(\frac{Re}{8})} \tag{13}$$

Where γ=0.577216 is the Euler's constant, Re is the Reynolds number, μ is the dynamic viscosity of the fluid, and u is the relative velocity of the particle with resp ect to the fluid.

Consider a particle moving in a microfluidic channel under the effect of acoustic ra diation force. When the inertia of a small particle in a viscous fluid is neglected, the force equation will have the form of

$$\sum \vec{F} = \overrightarrow{F_r} + \overrightarrow{F_d} = \vec{0} \tag{14}$$

where $\overrightarrow{F_r}$ is the acoustic radiation force acting on particle and $\overrightarrow{F_d}$ is the viscous drag force. If the general form of drag force in a Stokes flow is defined as $\overrightarrow{F_d} = -C\vec{u}$, where C is a coefficient depending on particle geometry and the surrounding fluid properties, equation (15) can be derived from (14) with the particle velocity $\vec{u}$. This equation gives the linear relationship between acoustic radiation force on particle and resulting velocity.

$$\overrightarrow{F_r} = C\vec{u} \tag{15}$$

$$\vec{u} = \frac{\overrightarrow{F_r}}{C}$$

CHAPTER 3

NUMERICAL EVALUATION OF ACOUSTIC RADIATION FORCE

3.1 Formulations and Numerical Evaluation Methodology

As given in the previous chapter, formula (4) is the general form of total acoustic radiation force acting on an object in an acoustic field. Acoustic radiation force calculation is based on integrating acoustic traction on a closed surface of S which can be either the object boundary or any surface encompassing that boundary. Acoustic radiation traction on the surface S is calculated from the first-order acoustic pressure and velocity fields, including both incident and scattered terms. Scattering effects from other surfaces in the vicinity as well as the scattering from the object surface are embedded in the first-order pressure and velocity terms p_1 and v_1. Therefore, this formulation also considers the secondary acoustic radiation forces which result from the acoustic particle-particle interactions or acoustic particle-wall interactions, in addition to the primary acoustic radiation force.

$$\overrightarrow{F_r} = -\int_S \left\{ \left[\frac{1}{2\rho_0 c_a^2} \langle p_1^2 \rangle - \frac{1}{2}\rho_0 \langle v_1^2 \rangle \right] \vec{n} + \rho_0 \langle (\vec{n} \cdot \overrightarrow{v_1}) \overrightarrow{v_1} \rangle \right\} dS \qquad (4)$$

Evaluation of the integral over an arbitrarily shaped surface S can render the calculation of acoustic radiation force possible in many cases, without previous restrictions. However, no analytical evaluation procedure to (4) exists without restrictions. Therefore numerical methods become crucial for the analyses of the cases outside of the restricted frame. By using numerical methods to solve the force integral, scope of the study can be extended, and the limitations brought by analytical formulations can be eliminated. Hence, this provides an opportunity for more detailed simulations and, therefore better understanding of acoustic manipulation of biological samples, which in many ways, contradicts with the previously mentioned assumptions.

Boundary Element Method is a numerical method to solve boundary value problem of a partial differential equation. A typical scheme consists of a domain inside or outside of a boundary [44]. Unlike the domain methods like FEM, Boundary element method (BEM) solves the governing PDE for the boundary first. Solution at a domain point is found later by the integration of known boundary data. Therefore, only boundary meshing is required for BEM, which brings computational ease compared to other domain methods. It is useful for far-field problems which include unbounded domain and bounded boundaries [45].Since it is based on the solution of the boundary integrals, it has better accuracy than FEM solutions on boundaries. For homogenous and isotropic fluid, the governing differential equation in acoustics is the linear wave equation: $\vec{r}_p$

$$\nabla^2\psi(\vec{r}_p, t) = \frac{1}{c^2}\frac{\partial^2}{\partial t^2}\psi(\vec{r}_p, t) \tag{16}$$

Where $\psi(p, t)$ is the velocity potential depending on spatial variable $\vec{r}_p$ and time t. c is the speed of sound in the fluid. By taking $\psi(\vec{r}_p, t)$ as the sum of real-valued harmonics, it is possible to reduce wave equation to Helmholtz equation

$$\nabla^2\emptyset(\vec{r}_p) + k^2\emptyset(\vec{r}_p) = 0 \tag{17}$$

where $\emptyset(\vec{r}_p)$ is the velocity potential independent of time, $k = {\omega_f}^2/c^2$ is wavenumber. Consider G_r as Green's function of Helmholtz equation. Y is the point on boundary $\partial\Omega$, X is the point in domain Ω where a solution is required. Integral equation becomes

$$C(X).\emptyset(X) + \int_{\partial\Omega}\emptyset(Y)\frac{\partial G_r}{\partial n_Y}(X,Y)ds(Y) = \int_{\partial\Omega}G_r\,(X,Y)\frac{\partial\emptyset}{\partial n_Y}(Y)ds(Y) \tag{18}$$

After boundary discretization, the integral is applied to all nodes on boundary and resulting system of equations is given as

$$(\boldsymbol{C}+\boldsymbol{H})[\emptyset]=\boldsymbol{G}\left[\frac{\partial\emptyset}{\partial n_Y}\right] \tag{19}$$

$\boldsymbol{C}$ is the matrix holding the geometry-dependent coefficient of the boundary element. **H** and **G** matrices are as given below.

$$\boldsymbol{H}\ \equiv\int_{\partial\Omega}\frac{\partial G_r}{\partial n_Y}(X\,,Y)\,ds(Y) \tag{20}$$

$$\boldsymbol{G}\ \equiv\int_{\partial\Omega}G_r(X\,,Y)\,ds(Y) \tag{21}$$

These equations can be rearranged to form a linear system of equations in the form of $A\Theta=\mathrm{B}$ where Θ vector contains information of $\emptyset$ and $\frac{\partial\emptyset}{\partial n_Y}$.

BEM method also has drawbacks. It is useful for linear partial differential equations but not available for non-linear problems. The solution to a non-homogenous system is not available by BEM method only. Therefore, it is coupled with FEM model when it is necessary to model the particle domain as another acoustic domain. For a particle in an acoustic field, the Helmholtz equation is solved using BEM and the first-order acoustic field obtained on fluid and particle boundaries. By using FEM for the particle domain, it is possible to include particle's response to the acoustic field. To couple BEM and FEM for such a model, pressure and normal velocity continuity is applied on the coupling boundary .

In this thesis, finite element and boundary element methods are used for the acoustic calculations via COMSOL Multiphysics. COMSOL Multiphysics software provides finite element method (FEM) and boundary element method (BEM) options for Pressure Acoustics module. In order to validate the use of these methods, simple cases are created in both 2D and 3D, which simply consists of an object in an acoustic field. The same case is simulated with different methods and couplings, and the results are compared to each other.

3.2 Validation of Results with Theory

In order to test the proposed numerical tool, three case studies are created. All of these cases include a single small particle in a large block that is filled with fluid. Particle is far from the walls, therefore in an approximately infinite domain. There exist analytical solutions for the acoustic force on small compressible spheres in plane acoustic wave. Case 1 is created for that configuration and to validate the numerical result with the analytical one. Apart from the spherical shape, non-spherical particle shape has to be validated, too. For non-spherical shape, there is Marston's formula for rigid oblate and prolate spheroids and Case 2 is designed based on this configuration. Case 1 and 2 apply to 3D and 2D axisymmetric models. With the computational load of 3D models, 2D axisymmetric option provides a chance to solve the problem in 2D where the resulting boundary integration can be extrapolated to 3D. However, 2D axisymmetric model lacks the opportunity for the cases with multiple particles unless they are all aligned in the symmetry axis. Therefore, the 2D cartesian model is a practical alternative suitable for multi-particle systems with much less computational load. Case 3 is created for only 2D cartesian models and their validation with the analytical results.

3.2.1 Case 1: Single Elastic Sphere

Case 1 is created to simulate a small compressible sphere in an acoustic field. Purpose of this case is to create a condition where Gorkov's analytical formulation is also valid for an isolated compressible sphere, therefore to test the ability of the proposed acoustic model. This case consists of a single spherical Polystyrene particle with 9 µm radius located at a specified point (x,y)=(0.75mm,0.25mm) in the rectangular channel, which has 1 mm width and 0.5 mm height. Channel is filled with water. In all of the models, Frequency Domain study was used at 750 kHz. Model geometry can be seen in Figure 3-1.

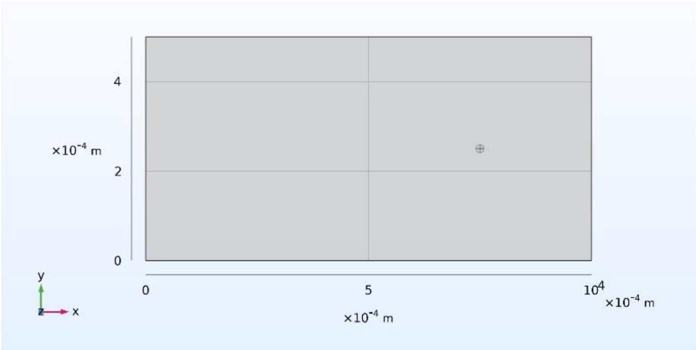

Figure 3-1 Case 1 model geometry

Acoustic field is created by the boundary acceleration, which is a simple representation of an ultrasonic actuator effect. Normal acceleration in x-direction is applied to the two vertical sidewalls with given parameter values so as to create a standing acoustic half-wave inside the channel. A standing half-wave will lead to maximum pressure amplitude on the walls and a minimum amplitude on the centerline of the channel. Therefore, a standing half-wave in a 1 mm width channel will have a wavelength of 0.5 mm in water, which requires a wave frequency of 750 kHz.

3.2.2 Case 2: Single Rigid Spheroid

Case 2 is created for validation of numerical results against analytical results for rigid, non-spherical particles. Similar to Case 1, there is a single particle in a block of 1mm width, 0.5 mm height and 0.6 mm depth, however it is a spheroidal particle this time. Particle is located at the same position as in Case 1, (x,y)=(0.75mm,0.25mm). For 3D models, the particle's z coordinate is determined as 0.3 mm, equally distant from walls in that direction. Unlike Case 1, spheroidal particle is modeled as a rigid particle since analytical results of King and Marston provide acoustic radiation force on rigid particles. Therefore, rigid particle case is used for validation of numerical methods here in order to use the numerical methods for elastic particles later.

Acoustic field is created via boundary acceleration of vertical walls and a standing half-wave is created in the x-direction inside the block. Acoustic radiation force is calculated by integrating the acoustic radiation traction on the particle surface. For the analytical counterpart, Marston's (10) formula is applied to the case. This formula depends on variation from spherical shape and provides a ratio of force on spheroid of eccentricity ε to force on a sphere of the same volume. Marston's formula for a perfect sphere also reduces to the King's (6) formula for acoustic force on small rigid spheres.

3.2.3 Case 3: Single Elastic Sphere in 2D

Computational load of 3D models can be challenging, hence two-dimensional models become useful as an alternative. 2D axisymmetric model is another useful tool that extrapolates line integrals to surface integrals by revolving the 2D geometry around an axis. However, for multiple-particle cases, it has limited opportunities. Considering all these, 2D cartesian model appears as a practical way for acoustic calculations. This case is mainly the two-dimensional version of Case 1. A single spherical polystyrene particle of 9 um radius is located at a rectangular block. A standing half-wave is created at x-direction via boundary acceleration. Acoustic radiation force is calculated at the circular boundary by the integration of acoustic radiation traction. The result of the integral is in N/m unit. Rectangular block with given parameters is modeled with a 2D rectangle. A spherical particle is represented in a 2D cartesian model with a circle. Both particle and fluid domains are modeled as linear elastic acoustic domains. In order to validate simulation results obtained by 2D cartesian models with both FEM and BEM-FEM coupled approaches, an analytical indicator is derived from Gorkov's formulation. Gorkov force is proportional to the particle volume and is used for validation of 3D simulation cases. However, in 2D cartesian simulation models, the particle is represented with a circular domain while the block is a rectangle. Therefore, acoustic radiation force is calculated with a line integral over the circular boundary in 2D, which gives results in N/m unit. Based on this, 2D simulations can be compared to the analytical force on the great circle of the 3D spherical particle. To obtain that, bracketed terms at Gorkov potential formulation can be multiplied by the area of the great circle instead of the volume of sphere. Gorkov's formulation for the force acting on the volume of particle, in Newton:

$$U_r = \frac{4\pi}{3} a^3 \left[f_1 \frac{1}{2\rho_0 c_a^2} \langle p_{in}^2 \rangle - f_2 \frac{3}{4} \rho_0 \langle v_{in}^2 \rangle \right] \tag{8}$$

$$\overrightarrow{F_r} = -\vec{\nabla} U_r \qquad [N]$$

To obtain the 2D force in N/m unit:

$$\frac{4\pi}{3} a^3 \rightarrow \pi a^2$$

$$U_r^* = \pi a^2 \left[f_1 \frac{1}{2\rho_0 c_a^2} \langle p_{in}^2 \rangle - f_2 \frac{3}{4} \rho_0 \langle v_{in}^2 \rangle \right] \tag{22}$$

$$\overrightarrow{F_r^*} = -\vec{\nabla} U_r^* \qquad [N/m]$$

For 1D standing plane wave:

$$\bar{F}^{rad} = 3\pi k a^2 E_{ac} \Phi \sin(2kx) \qquad [N/m\,] \tag{23}$$

3.3 FEM Based Approach

In this approach, both particle and surrounding fluid domains are modeled as acoustic domains with finite element method. By modeling the particle as an acoustic domain, it is considered as a fluid particle, which is a special case of an elastic particle without any shear effect. COMSOL Multiphysics provides 3D cartesian, 2D cartesian, and 2D axisymmetric model options, and these three are used to model the verification cases with the FEM approach.

3.3.1 3D FEM Model: Case 1

Geometry consists of a sphere in a rectangular block representing the particle and surrounding fluid domains. Both particle and fluid domains are modeled with Pressure Acoustics, Frequency Domain (FEM) physics. Actuation is provided by boundary acceleration of the walls shown in Figure 3-2. The resulting pressure field is found by solving Helmholtz Equation for given frequency, and acoustic radiation force on the particle is found by integrating acoustic traction over particle surface. Both domains are modeled as linear elastic and meshed with tetrahedral elements. Model parameters are given in Table 3-1.

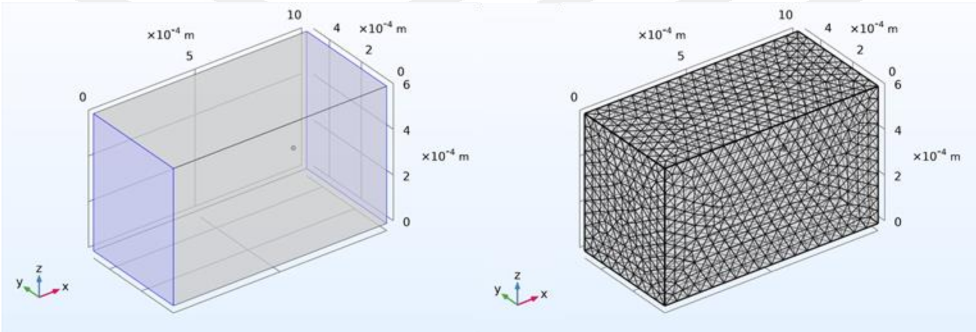

Figure 3-2 Model geometry and mesh

Table 3-1 Model parameters for FEM approach/Case1

Parameter	Value
Particle density	1060 kg/m^3
Particle speed of sound	2350 m/s
Particle Radius	9 μm
Mesh size (particle boundary)	0.4 μm, 2 μm (max)
Particle position	(x,y,z)=(0.75 mm, 0.25 mm, 0.3 mm)
Fluid domain dimensions	1mm x 0.5 mm x 0.6 mm
Fluid density	998.25 kg/m^3
Fluid speed of sound	1500 m/s
Mesh size (fluid domain)	60 μm (max)
Frequency	750 kHz
Wavelength in fluid	2 mm

First-order pressure field created in the block due to boundary acceleration is given in

Figure 3-3 Figure 3-3 (a) below, and the pressure on the particle boundary is given in (b). A standing half-wave with a pressure amplitude of 106.04 kPa is created in the x-direction of the block. Acoustic radiation force is calculated by both integration over particle boundary (4) and analytical formulation (9), which uses pressure amplitude inside the block as an input. Results are given in Table 3-2 below. When compared to the analytical solution of that specific conditions, it is seen that the numerical model comes with a 0.055% error. Therefore, it can be concluded that the 3D FEM based approach can be used for numerical simulations.

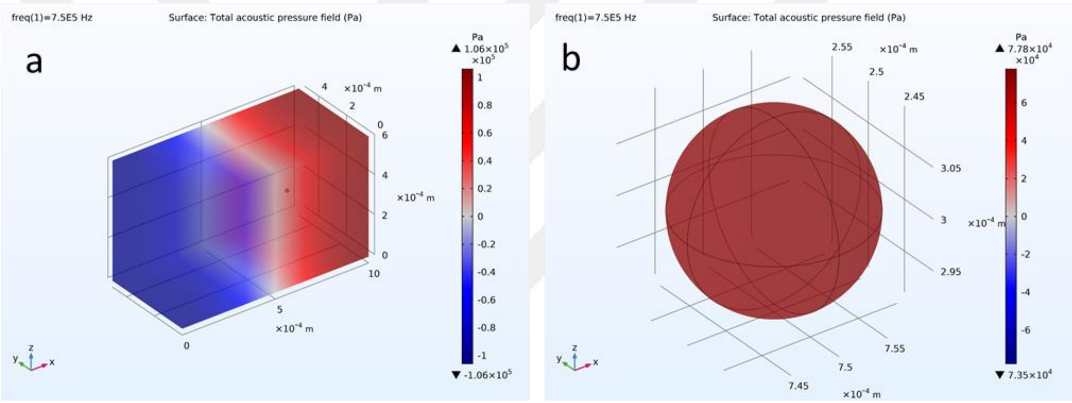

Figure 3-3 Resulting acoustic pressure field in the block (a), Acoustic pressure field on the particle (b)

Table 3-2 Model results FEM approach: Case 1

3D FEM-FEM Approach: Case 1 Results	
Pressure Amplitude	106.04 kPa
Maximum pressure on particle	77.838 kPa
Minimum pressure on particle	73.504 kPa
Computation time	19 s
Acoustic radiation force (FEM)	-8.5302 pN
Acoustic radiation force (Gorkov's Analytical)	-8.5255 pN
Error	0.055 %

3.3.2 3D FEM Model: Case 2

For this case, the particle is modeled as a spheroid of the same volume with a sphere of 9 um radius. The particle is assumed as rigid. Geometry consists of a block and a spheroidal particle inside it. Both oblate and prolate cases are considered with a major axis radius is 1.5 times the minor axis radius. The spheroid is located at a point at $\lambda/8$ distance from the pressure nodal line. Acoustic wave is created in the x-direction along the symmetry axis of the spheroid. To simulate rigid particle surface, particle domain is not modeled with pressure acoustics. Therefore particle boundary is automatically treated as a sound hard wall with zero acoustic velocity. Model parameters are given in Table 3-3.

Table 3-3 Model parameters FEM approach/Case 2

Parameter	Value
Oblate spheroid dimensions	R_x= 6.8683 µm R_y=R_z=10.3024 µm
Oblate spheroid shape parameter	ε= 0.5
Prolate spheroid dimensions	R_x= 11.7933 µm R_y=R_z=7.8622 µm
Prolate spheroid shape parameter	ε= -0.33
Equivalent Sphere Radius	9 µm
Mesh size (particle boundary)	0.7 µm, 2 µm (max)
Particle position	(x,y,z)=(0.75 mm, 0.25 mm, 0.3 mm)
Fluid domain dimensions	1mm x 0.5 mm x 0.6 mm
Fluid density	998.25 kg/m^3
Fluid speed of sound	1500 m/s
Mesh size (fluid domain)	60 µm (max)
Frequency	750 kHz
Wavelength in fluid	2 mm

Resulting first-order acoustic pressure distribution in the block and on the particle surface is for both oblate, and prolate spheroid cases are given below (Figure 3-4). Acoustic radiation force integrals are calculated over particle surface and compared to the Marston's analytical formula for rigid spheroids. For rigid oblate spheroid, the numerical result of acoustic radiation force differs from analytical result by 0.1788 % error, and for prolate spheroid, the difference from analytical solution is 0.1187

%, as can be seen in Table 3-4. Same mesh settings are used for both cases. It can also be noted that the case of a rigid sphere is also simulated numerically, and result is compared to Marston's formula which converges to King's formula for rigid spheres. 0.1673 % difference between 3D FEM simulation and analytical formulation is obtained.

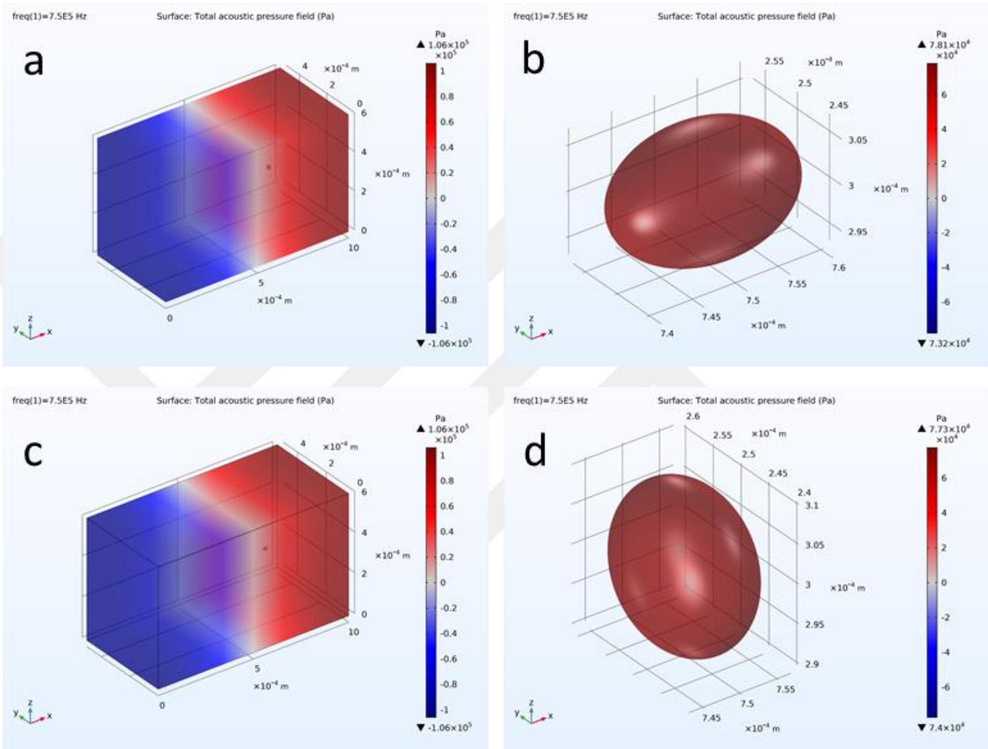

Figure 3-4 Resulting acoustic pressure field on oblate spheroid (d) and prolate spheroid (b), Acoustic pressure field in the block(a),(c)

Table 3-4 Model results FEM approach/Case 2

3D FEM Approach: Case 2 Results for Rigid Oblate Spheroid	
Pressure Amplitude	105.98 kPa
Maximum pressure on particle	78.549 kPa
Minimum pressure on particle	72.698 kPa
Computation time	17 s
Acoustic radiation force (FEM)	-34.8312 pN
Acoustic radiation force (Marston’s Analytical)	-34.8936pN
Error	0.1788 %
3D FEM Approach: Case 2 Results for Rigid Prolate Spheroid	
Pressure Amplitude	106.00kPa
Maximum pressure on particle	79.229 kPa
Minimum pressure on particle	71.972 kPa
Computation time	22 sn
Acoustic radiation force (FEM)	-28.6665 pN
Acoustic radiation force (Marston's Analytical)	-28.6325 pN
Error	0.1187 %

3.3.3 2D Axisymmetric FEM Model: Case 1

An elastic spherical particle is modeled.Both particle and fluid domains are modeled with Pressure Acoustics, Frequency Domain (FEM) physics. Geometry is arranged such that r=0 is the symmetry axis. In this case, normal acceleration is applied to the horizontal walls. Domains are meshed with Free Triangular. Model geometry and mesh around the particle boundary is shown in Figure 3-5. Model parameters are given in Table 3-5. Acoustic radiation force integral is calculated over revolved particle geometry (Table 3-6). Results are given in Figure 3-6 and Table 3-6.

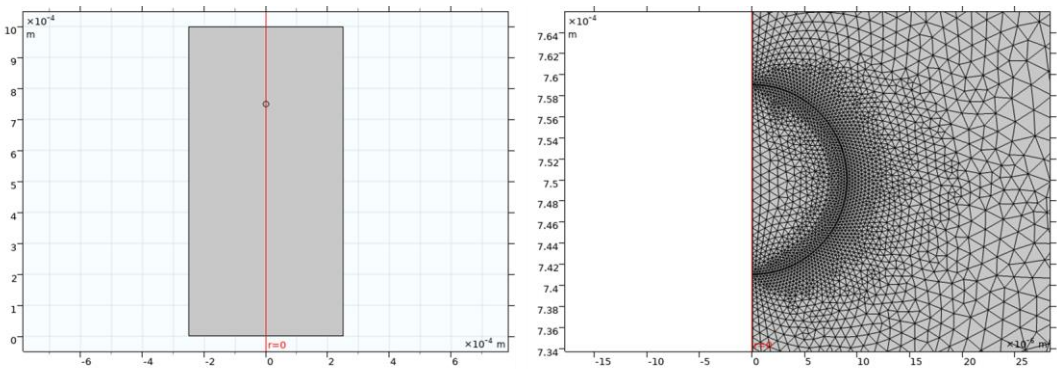

Figure 3-5 2D Axisymmetric model geometry and meshing around particle

Table 3-5 Model parameters 2D axisymmetric/Case 1

Parameter	Value
Particle density	1060 kg/m^3
Particle speed of sound	2350 m/s
Particle Radius	9 µm
Mesh size (particle boundary)	0.4 µm, 2 µm (max)
Particle position	(r,z)=(0 mm, 0.75 mm)
Fluid domain dimensions	R=0.25 mm, h=1 mm
Fluid density	998.25 kg/m^3
Fluid speed of sound	1500 m/s
Mesh size (fluid domain)	10 µm (max)
Frequency	750 kHz
Wavelength in fluid	2 mm

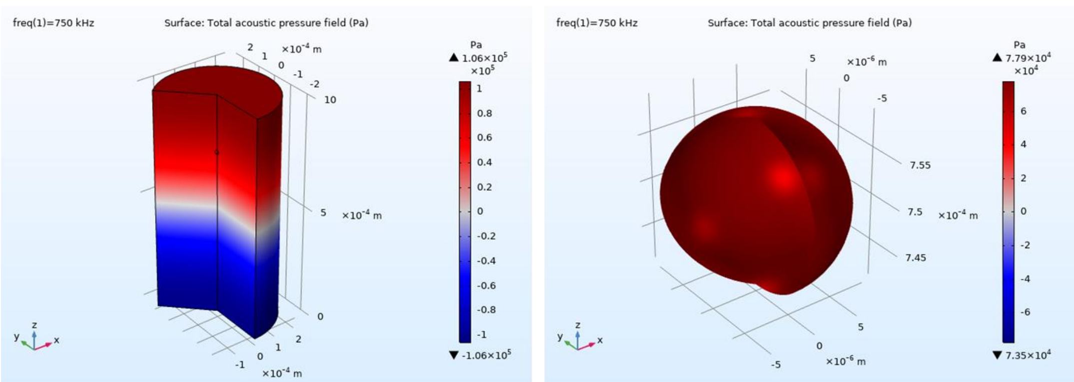

Figure 3-6 Resulting acoustic pressure distribution on fluid domain and particle

Table 3-6 Model results 2D axisymmetric/ Case 1

2D Axisymmetric FEM-FEM Approach: Case 1 Results	
Pressure Amplitude	106.05 kPa
Maximum pressure on particle	77.846kPa
Minimum pressure on particle	73.512kPa
Computation time	3 s
Acoustic radiation force (FEM)	-8.6749 pN
Acoustic radiation force (Gorkov's Analytical)	-8.5271 pN
Error	1.7333 %

3.3.4 2D Axisymmetric FEM Model: Case 2

Rigid oblate and prolate spheroids are modeled in a 1D standing half-wave at z-direction, which is the vertical direction in 2D axisymmetric Model. Surrounding fluid is a linear elastic domain with acoustic properties of water. Particle domain is not modeled with Pressure acoustics; therefore, fixed particle boundary of a rigid particle is simulated with sound hard wall boundary condition on the particle surface. Model parameters are given in Table 3-7below. Particle boundary is meshed densely and the same settings are used for both oblate and prolate spheroid cases. Meshing close to particle boundaries is given in Figure 3-7. Revolved geometries are given in Figure 3-8. Acoustic radiation force integral is calculated over revolved particle surface. Numerically calculated forces at z-direction are compared to Marston's analytical formula. Results are given in Table 3-8.

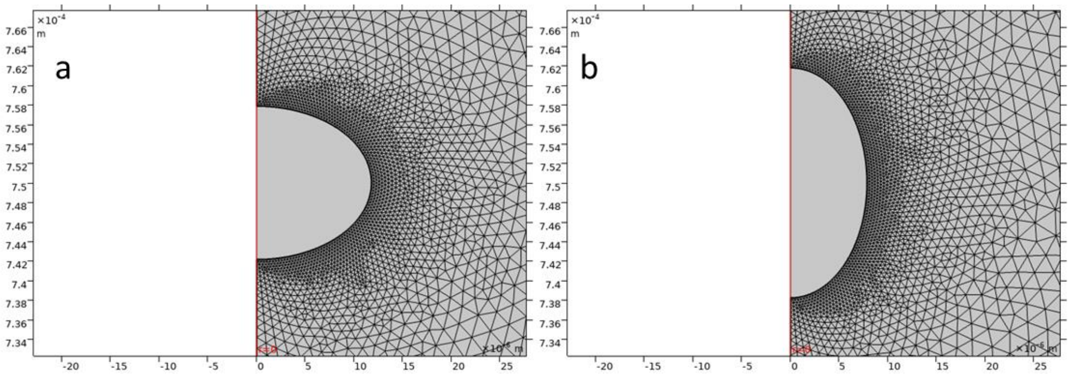

Figure 3-7 Meshing around particle boundary for oblate (a) and prolate (b) spheroids.

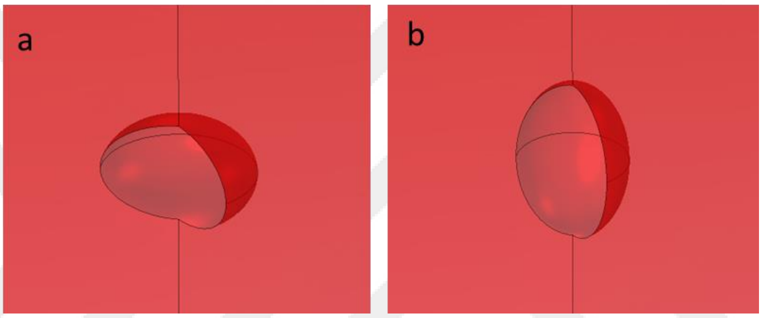

Figure 3-8 Oblate (a) and prolate (b) spheroids revolved geometries

Table 3-7 Model parameters 2D axisymmetric/ Case2

Parameter	**Value**
Oblate spheroid dimensions	R_r= 6.8683 μm R_z=10.3024 μm
Oblate spheroid shape parameter	ε= 0.5
Prolate spheroid dimensions	R_r= 11.7933 μm R_z=7.8622 μm
Prolate spheroid shape parameter	ε= -0.33
Equivalent Sphere Radius	9 μm
Mesh size (particle boundary)	0.3 μm
Particle position	(r,z)=(0 mm, 0.75 mm)
Fluid domain dimensions	1mm x 0.5 mm x 0.6 mm
Fluid density	998.25 kg/m^3
Fluid speed of sound	1500 m/s
Mesh size (fluid domain)	10 μm (max)
Frequency	750 kHz
Wavelength in fluid	2 mm

Table 3-8Model results 2D axisymmetric/Case 2

3D FEM Approach: Case 2 Results for Rigid Oblate Spheroid	
Pressure Amplitude	105.966 kPa
Maximum pressure on particle	78.535kPa
Minimum pressure on particle	72.685 kPa
Computation time	3 s
Acoustic radiation force (FEM)	-34.8961 pN
Acoustic radiation force (Marston’s Analytical)	-34.8712pN
Error	0.0714 %
3D FEM Approach: Case 2 Results for Rigid Prolate Spheroid	
Pressure Amplitude	105.995 kPa
Maximum pressure on particle	79.225 kPa
Minimum pressure on particle	71.967 kPa
Computation time	3 sn
Acoustic radiation force (FEM)	-28.6588 pN
Acoustic radiation force (Marston's Analytical)	-28.6298 pN
Error	0.1013 %

3.3.5 2D Cartesian FEM Model: Case 3

Rectangular block and the circular particle geometry is created. Both domains are are linear elastic acoustic domains. Free triangular mesh is used for both domains. Actuation is provided via acceleration of two vertical channel walls. Frequency domain at 750 kHz is run. First-order acoustic field is obtained as shown in Figure 3-9 and acoustic radiation force on the particle is calculated by integration over the particle boundary line. Model parameters are given in Table 3-9 and results are given in Table 3-10.

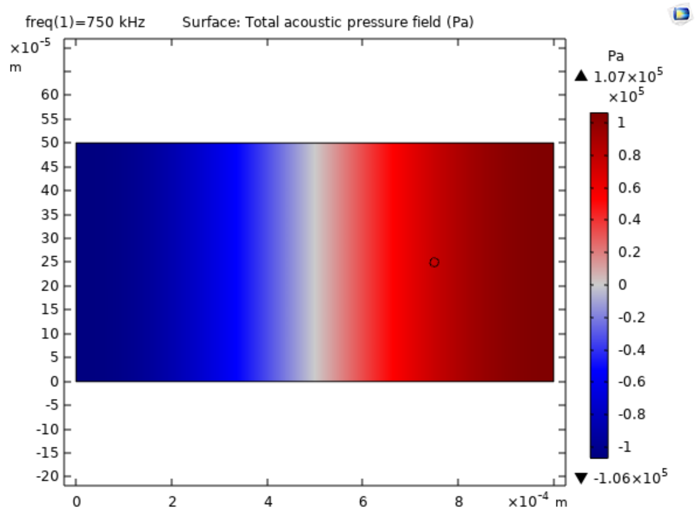

Figure 3-9 Resulting acoustic pressure field FEM approach/Case3

Table 3-9 Model parameters 2D cartesian FEM approach/Case 3

Parameter	**Value**
Particle density	1060 kg/m^3
Particle speed of sound	2350 m/s
Particle Radius	9 µm
Mesh size (particle boundary)	0.3 µm, 1 µm (max)
Particle position	(x,y)=(0.75 mm, 0.25 mm)
Fluid domain dimensions	1 mm x 0.5 mm
Fluid density	998.25 kg/m^3
Fluid speed of sound	1500 m/s
Fluid Mesh size	20 µm (max)
Frequency	750 kHz
Wavelength in fluid	2 mm

Table 3-10 Model results 2D cartesian FEM approach/Case 3

2D Cartesian FEM-FEM Approach: Case 3 Results	
Pressure Amplitude	106.550 kPa
Maximum pressure on particle	78.184 kPa
Minimum pressure on particle	73.786 kPa
Computation time	3 s
Acoustic radiation force (FEM)	-7.1797 10^{-7} N/m
Acoustic radiation force (Gorkov's Analytical)	-7.1731 10^{-7} N/m
Error	0.092 %

3.4 BEM Based Approach

Previously designed cases are simulated using Boundary Element Method (BEM) and for elastic particle cases, it is coupled with Finite Element Method (FEM) to simulate the elastic particle domain in addition to the surrounding fluid domain. BEM is used to find the acoustic pressure field at fluid boundaries, and therefore at the particle boundary, while FEM is used to simulate the acoustic domain inside the elastic particle. Two methods are coupled in terms of the equality of acoustic pressure and normal velocity components on particle boundary. For rigid particle cases, particle domain is not modelled as an acoustic domain and particle boundary is treated as a sound-hard wall. Therefore only BEM is used for these cases.

3.4.1 3D BEM-FEM Coupled Approach: Case 1

A rectangular block of 1 mm width, 0.5 mm height and 0.6mm depth is created to represent a volume of a microchannel. A spherical geometry is located at a point of (x,y,z)=(0.75 mm, 0.25 mm, 0.3 mm). Fluid domain is modeled with BE Method and the particle domain is modelled with FE Model. Particle is an elastic sphere of 9 um radius. A planar standing half wave is created via boundary acceleration along the width of the channel. Acoustic radiation force is calculated by integrating on particle boundary. Model parameters are given in Table 3-11. Resulting pressure distribution on block and particle boundaries are given in Figure 3-10 below. Results of boundary integration is given in Table 3-12.

Table 3-11 Model parameters 3D BEM-FEM approach/Case 1

Parameter	**Value**
Particle density	1060 kg/m^3
Particle speed of sound	2350 m/s
Particle Radius	9 μm
Mesh size (particle boundary)	1 μm, 2 μm (max)
Particle position	(x,y,z)=(0.75 mm, 0.25 mm, 0.3 mm)
Fluid domain dimensions	1mm x 0.5 mm x 0.6 mm
Fluid density	998.25 kg/m^3
Fluid speed of sound	1500 m/s
Mesh size (fluid boundary)	60 μm (max)
Frequency	750 kHz
Wavelength in fluid	2 mm

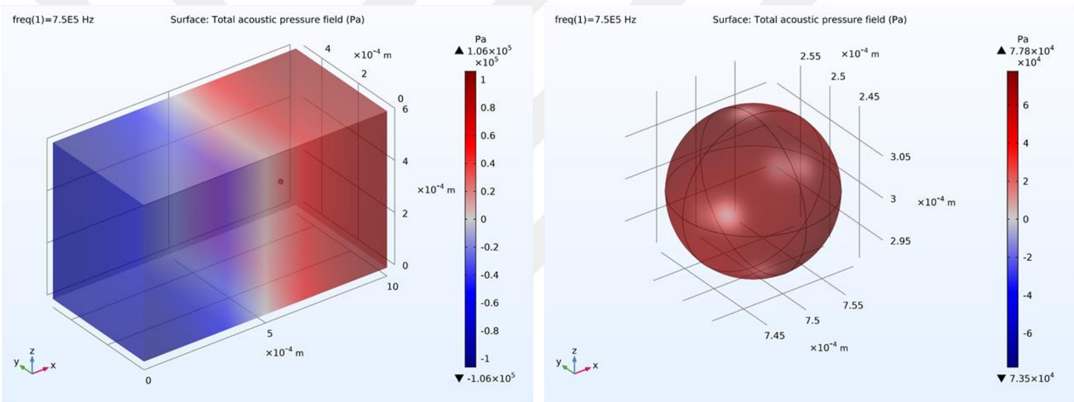

Figure 3-10 Block and particle geometries

Table 3-12 Model results 3D BEM-FEM approach/Case 1

3D BEM-FEM Coupled Approach: Case 1 Results	
Pressure Amplitude	106.07 kPa
Maximum pressure on particle	77.8198kPa
Minimum pressure on particle	73.4871 kPa
Computation time	23 s
Acoustic radiation force (BEM-FEM)	-8.5276 pN
Acoustic radiation force (Gorkov's Analytical)	-8.5304 pN
Error	0.032 %

3.4.2 3D BEM Based Approach: Case 2

In this case, a rigid spheroidal particle is located at a point in a rectangular block. Block dimensions and the location of the particle in the block are the same as in the Case 1. To simulate a rigid spheroid, particle boundary is treated as a fixed surface by sound-hard wall condition. Fluid domain is modeled as water. Both oblate and prolate spheroid shapes, which have the same volume as a sphere of 9 um radius, are tested. For both prolate and oblate cases, spheroids are located in the block such that their symmetry axes are on x-axis, aligned with the acoustic wave direction. In order to compare the numerical results to analytical results, Marston's analytical formula for a rigid spheroid is used. Model parameters are given in Table 3-13. Resulting pressure distribution on particle and block surfaces are given in Figure 3-11 and the numerical force with the analytical counterpart is given in Table 3-14.

Table 3-13 Model parameters for 3D BEM based approach/ Case 2

Parameter	Value
Oblate spheroid dimensions	R_x= 6.8683 µm R_y=R_z=10.3024 µm
Oblate spheroid shape parameter	ε= 0.5
Prolate spheroid dimensions	R_x= 11.7933 µm R_y=R_z=7.8622 µm
Prolate spheroid shape parameter	ε= -0.33
Equivalent Sphere Radius	9 µm
Mesh size (particle boundary)	2 µm (max)
Particle position	(x,y,z)=(0.75 mm, 0.25 mm, 0.3 mm)
Fluid domain dimensions	1mm x 0.5 mm x 0.6 mm
Fluid density	998.25 kg/m^3
Fluid speed of sound	1500 m/s
Mesh size (fluid oundary)	60 µm (max)
Frequency	750 kHz
Wavelength in fluid	2 mm

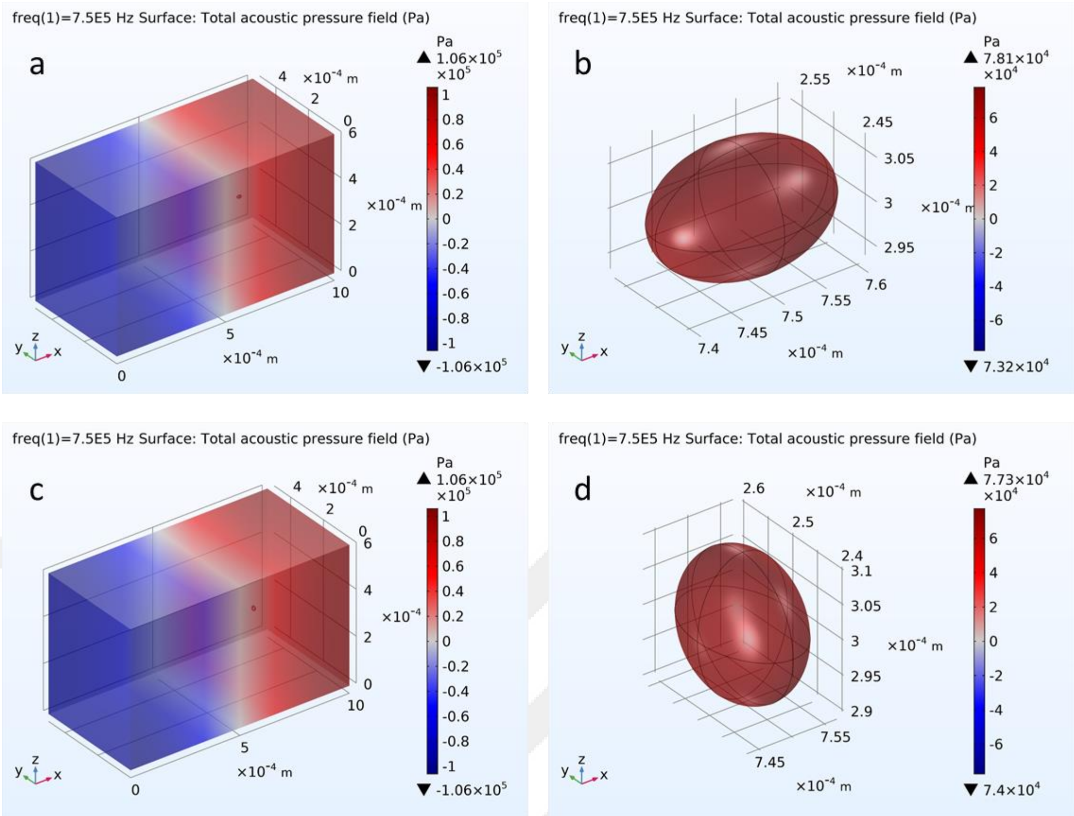

Figure 3-11 Resulting acoustic pressure field on oblate spheroid (d) and prolate spheroid (b), Acoustic pressure field in the block(a),(c)

Table 3-14 Model results for 3D BEM based approach/ Case 2

3D BEM Approach: Case 2 Results for Rigid Oblate Spheroid	
Pressure Amplitude	106.015kPa
Maximum pressure on particle	78.528 kPa
Minimum pressure on particle	72.679 kPa
Computation time	36 s
Acoustic radiation force (BEM)	-34.9254 pN
Acoustic radiation force (Marston’s Analytical)	-34.8936pN
Error	0.0888 %
3D FEM Approach: Case 2 Results for Rigid Prolate Spheroid	
Pressure Amplitude	106.036 kPa
Maximum pressure on particle	79.211 kPa
Minimum pressure on particle	71.956 kPa
Computation time	32 sn
Acoustic radiation force (FEM)	-28.6305 pN
Acoustic radiation force (Marston's Analytical)	-28.6325 pN
Error	0.007 %

3.4.3 2D BEM-FEM Coupled Approach: Case 3

Single circular geometry of 9 µm radius is located in a rectangle of 1mm width and 0.5 mm height. The circle is modelled as an acoustic field and solved via FE method while remaining area of rectangle is modeled with BE Method. Acoustic half-wave is created in x direction (Figure 3-12Figure 3-12). Acoustic traction is integrated over circular boundary and result is compared to 2D Approximation of Gorkov's analytical model .model parameters are in Table 3-15 and calculated force values are in Table 3-16.

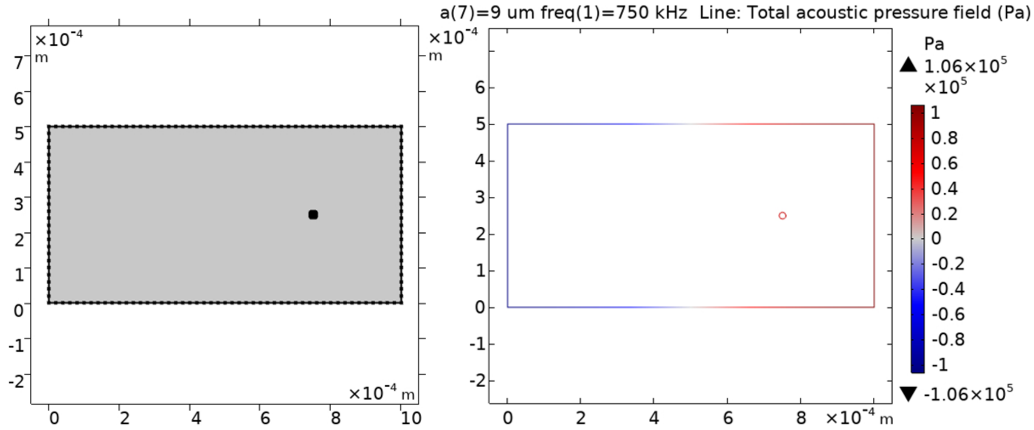

Figure 3-12 2D cartesian BEM-FEM model/Case 3

Table 3-15 Model parameters 2D cartesian BEM-FEM/Case 3

Parameter	**Value**
Particle density	1060 kg/m^3
Particle speed of sound	2350 m/s
Particle Radius	9 µm
Mesh size (particle boundary)	1 µm, 2 µm (max)
Particle position	(x,y)=(0.75 mm, 0.25 mm)
Fluid domain dimensions	1 mm x 0.5 mm
Fluid density	998.25 kg/m^3
Fluid speed of sound	1500 m/s
Mesh size (fluid boundary)	20 µm (max)
Frequency	750 kHz
Wavelength in fluid	2 mm

Table 3-16 Model results 2D cartesian BEM-FEM/Case 3

2D Cartesian BEM-FEM Approach: Case 3 Results	
Pressure Amplitude	106.504kPa
Maximum pressure on particle	78.149kPa
Minimum pressure on particle	73.754 kPa
Computation time	7 s
Acoustic radiation force (BEM-FEM)	-7.1797 10^{-7} N/m
Acoustic radiation force (Gorkov's Analytical)	-7.1731 10^{-7} N/m
Error	0.092 %

3.5 Calculation of Drag Force

3.5.1 Drag Force on an Isolated Particle

In order to calculate the trajectory of a particle under acoustic radiation force effect, drag force on the particle must be known. As mentioned in earlier chapters, inertial effects are neglected; therefore, particle is assumed to travel at a constant speed in a time increment. FEM based numerical model is developed to calculate drag force on an arbitrarily shaped particle moving with a constant speed relative to the fluid. This model can be extended to multiple particle case in which hydrodynamic interactions between particles are also included. Therefore, drag force calculation for multiple, finite-sized particles can be obtained.

The analytical scheme given above is used for the validation of the FEM based models developed for calculating viscous drag force. Following cases are created for validation of the numerical method to the analytical methods given in section 2.2. Single rigid spherical particle and single rigid ellipsoid shapes are modeled using 2D axisymmetric model, while 2D cartesian model is used for the rigid cylinder of unit length.

2D axisymmetric model with FEM based Creeping flow module is used to calculate drag force numerically for a spherical particle case. A spherical particle of 3 μm radius on the center of a cylindrical block of 1 mm diameter and 2 mm height is modeled for axisymmetric model. Surrounding fluid is water and a unit velocity in z-direction is defined on the particle boundary. A stationary study is run, and the velocity and pressure fields are obtained. To find the total drag force acting on particle, total stress component in the z-direction is integrated over particle surface.

Particle is assumed isolated since the distance from the walls is more than 20 diameter. Stokes drag formula (11) is used for comparison. Parameters and results are given in Table 3-17. Numerical results and corresponding analytical results are in good agreement.

Table 3-17Model parameters and results /Sphere

Parameter	**Value**
Fluid dynamic viscosity: μ	0.89e-3 Pa.s
Sphere radius: R	3 μm
Sphere velocity: u	1 m/s
Analytical:	F_{drag}=5.0328e-8 N
2D-axisymmetric model:	F_{drag}=5.0665e-8 N
Error:	0.6696 %

Table 3-18 Model parameters and results /Spheroid

Parameter	**Prolate Spheroid**	**Oblate Spheroid**
Radius along symmetry axis: a	3 μm	1 μm
Radius perpendicular to symmetry axis: b	1 μm	3 μm
Shape coefficient: C_v (Lai&Mockros)	1.4045	0.8787
Velocity: u	1 m/s	1 m/s
Drag Force	**Prolate Spheroid**	**Oblate Spheroid**
2D-axisymmetric model:	2.3574e-8 N	4.4104e-8 N
Analytical:	2.3562e-8 N	4.4224e-8 N
Error:	0.05 %	0.27 %

Another case for validation is the spheroid case. Drag force on a rigid spheroid moving along its symmetry axis was given in (12). In order to simulate this case, a numerical scheme of the previous case is used, however, with a prolate spheroid of R_r=1 μm and R_z=3 μm and an oblate spheroid of R_r=3 μm and R_z=1 μm located at the center of the cylindrical block. Same procedure applied to this case and the results are compared to Lai and Mockros's formula. Parameter values and results are given in Table 3-18.

For the last case, a rigid cylinder of unit length is modelled using 2D cartesian model. The cylinder of unit length is represented by a circle of 5 um radius, which has a unit velocity at x-direction with respect to the fluid inside of a rectangle of 0.4 mm width and 0.3 mm height. Results are given in Table 3-19. The same study was repeated for cylinder radius values from 1 um to 15 um and the error between analytical and numerical results remained under 1 % at each radius.

Table 3-19 Model parameters and results /Unit-length cylinder

Parameter	**Value**
Fluid viscosity: μ	0.89e-3 Pa.s
Sphere radius: R	5 μm
Sphere velocity: u	1 m/s
Drag force	**Value**
Analytical (Lamb):	F_{drag}=2.5153e-11 N
2D-cartesian model:	F_{drag}=2.5107e-11 N
Error:	0.1829 %

3.5.2 Drag Force Including Hydrodynamic Interactions

Based on the FEM model used for isolated particles, a new model and an integrated methodology is created to calculate the drag force exerted on particles due to the movement inside the microfluidic channel. This method, unlike the previous one, also includes the hydrodynamic effects of other particles or walls around. There is no limitation on particle geometry. The whole configuration of channel walls and all particles are modeled in the FEM model at the same time. The method is explained below for a simple case of two elliptical particles inside a closed cavity filled with water. To calculate the velocity of particles due to acoustic forces, resistance matrix L_H is required. Resistance matrix keeps the effects of all particles and walls to each particle. To obtain that matrix, unit velocity in both translational directions and a unit rotational velocity is defined on each particle one by one, and resulting effects on all particles due to that unit velocity are calculated, and results create a column of the resistance matrix.

$$\sum \vec{F} = \vec{F}^{acoustic} + \vec{F}^{drag} = \vec{0}$$

$$[L_H][v] = \vec{F}^{acoustic} = -\vec{F}^{drag}$$

$$\begin{array}{c}
\begin{array}{cccccc} v_x^1 & v_y^1 & w^1 & v_x^2 & v_y^2 & w^2 \\ \downarrow & \downarrow & \downarrow & \downarrow & \downarrow & \downarrow \end{array} \\
\begin{bmatrix} L_{11} & L_{12} & L_{13} & L_{14} & L_{15} & L_{16} \\ L_{21} & L_{22} & L_{23} & L_{24} & L_{25} & L_{26} \\ L_{31} & L_{32} & L_{33} & L_{34} & L_{35} & L_{36} \\ L_{41} & L_{42} & L_{43} & L_{44} & L_{45} & L_{46} \\ L_{51} & L_{52} & L_{53} & L_{54} & L_{55} & L_{56} \\ L_{61} & L_{62} & L_{63} & L_{64} & L_{65} & L_{66} \end{bmatrix}
\end{array}
\begin{bmatrix} v_x^1 \\ v_y^1 \\ w^1 \\ v_x^2 \\ v_y^2 \\ w^2 \end{bmatrix} = \begin{bmatrix} F_x^1 \\ F_y^1 \\ T^1 \\ F_x^2 \\ F_y^2 \\ T^2 \end{bmatrix}$$

Let the positions of the two particles be as follows:

Particle 1 position : (x_0^1, y_0^1)

Particle 2 position: (x_0^2, y_0^2)

1st column of L_H matrix:

Define unit velocity in x-direction to the first particle and keep the second particle fixed and run the simulation. Effect of unit x-velocity of the first particle on both particles is the first column of the matrix. σ_x, σ_y refers to the x and y components of total hydrodynamic stresses while Γ_1, Γ_2 refers to the boundaries of particle 1 and particle 2.

Particle 1: $\begin{bmatrix} v_x & v_y \end{bmatrix} = [1 \quad 0]$ [m/s]

Particle 2: $\begin{bmatrix} v_x & v_y \end{bmatrix} = [0 \quad 0]$ [m/s]

$$L_{11} = \int_{\Gamma_1,} \sigma_x \, . \, ds \qquad at\ particle\ 1\ \ boundary$$

$$L_{21} = \int_{\Gamma_1,} \sigma_y \, . \, ds \qquad at\ particle\ 1\ \ boundary$$

$$L_{31} = \int_{\Gamma_1,} \left((x - x_0^2) * \sigma_y - (y - y_0^2) * \sigma_x\right) ds \qquad at\ particle\ 1\ \ boundary$$

$$L_{41} = \int_{\Gamma_2,} \sigma_x \, . \, ds \qquad at\ particle\ 2\ \ boundary$$

$$L_{51} = \int_{\Gamma_2,} \sigma_y \, . \, ds \qquad at\ particle\ 2\ \ boundary$$

$$L_{61} = \int_{\Gamma_2,} \left((x - x_0^2) * \sigma_y - (y - y_0^2) * \sigma_x\right) ds \qquad at\ particle\ 2\ \ boundary$$

2nd column of L_H matrix:

Define unit velocity at y-direction to the first particle and keep the second one fixed. Resulting effects on both particles constitute the second column of matrix.

Particle 1: $\begin{bmatrix} v_x & v_y \end{bmatrix} = [0 \quad 1]$ [m/s]

Particle 2: $\begin{bmatrix} v_x & v_y \end{bmatrix} = [0 \quad 0]$ [m/s]

$$L_{12} = \int_{\Gamma_{1},} \sigma_x \,.\, ds \qquad at\ particle\ 1\ \ boundary$$

$$L_{22} = \int_{\Gamma_{1},} \sigma_y \,.\, ds \qquad at\ particle\ 1\ \ boundary$$

$$L_{32} = \int_{\Gamma_{1},} \Big((x - x_0^2) * \sigma_y - (y - y_0^2) * \sigma_x\Big)\, ds \qquad at\ particle\ 1\ \ boundary$$

$$L_{42} = \int_{\Gamma_{2},} \sigma_x \,.\, ds \qquad at\ particle\ 2\ \ boundary$$

$$L_{52} = \int_{\Gamma_{2},} \sigma_y \,.\, ds \qquad at\ particle\ 2\ \ boundary$$

$$L_{62} = \int_{\Gamma_{2},} \Big((x - x_0^2) * \sigma_y - (y - y_0^2) * \sigma_x\Big)\, ds \qquad at\ particle\ 2\ \ boundary$$

3rd column of L_H matrix:

Define unit rotational velocity to first particle only and keep the second particle fixed. Resulting effects on both particles are the third column of the matrix.

Particle 1: $[v_x \quad v_y] = [(y_0^1 - y) \quad (x - x_0^1)]$ [m/s]

Particle 2: $[v_x \quad v_y] = [0 \quad 0]$ [m/s]

$$L_{13} = \int_{\Gamma_{1},} \sigma_x \,.\, ds \qquad at\ particle\ 1\ \ boundary$$

$$L_{23} = \int_{\Gamma_{1},} \sigma_y \,.\, ds \qquad at\ particle\ 1\ \ boundary$$

$$L_{33} = \int_{\Gamma_1,} \left((x - x_0^2) * \sigma_y - (y - y_0^2) * \sigma_x\right) ds \qquad at\, particle\ 1\ \ boundary$$

$$L_{43} = \int_{\Gamma_2,} \sigma_x \,.\, ds \qquad at\, particle\ 2\ \ boundary$$

$$L_{53} = \int_{\Gamma_2,} \sigma_y \,.\, ds \qquad at\, particle\ 2\ \ boundary$$

$$L_{63} = \int_{\Gamma_2,} \left((x - x_0^2) * \sigma_y - (y - y_0^2) * \sigma_x\right) ds \qquad at\, particle\ 2\ \ boundary$$

The previous three steps are repeated however, this time the first particle is kept fixed, and the second particle has unit velocities in three degrees of freedom one by one. Similar procedure is applied and the remaining three columns are obtained.

After the resistance matrix is constructed, velocities can be calculated for any configuration by the following formula

$$[v] = [L_H]^{-1}[F^{acoustic}]$$

In this chapter, numerical models for both acoustic and hydrodynamic parts are introduced. Three simple cases are created for acoustic simulations corresponding to a compressible sphere, a rigid spheroid, and a compressible spherical particle in 2D. Numerical results are compared to the related analytical solutions for 3D, 2D axisymmetric, and 2D cartesian models. Among all simulations, the maximum error between numerical and the corresponding analytical result occurred as 1.74% for 2D axisymmetric model with FEM approach in Case 1. Other than that, the error values of all remaining simulations are less than 0.2%. Based on this comparison, it is concluded that the numerical results are in good agreement with the analytical results for the acoustic part, therefore numerical tool can be used to calculate acoustic radiation force . A FEM based model is designed to calculate hydrodynamic viscous drag on arbitrarily-shaped particle moving inside a fluid. This numerical tool is verified against the existing analytical solutions for a sphere, a spheroid and a cylinder of unit length. Again, difference between numerical and analytical results does not exceed 0.7% for all cases in this part. Therefore, proposed numerical tool gives results in good agreement with the analytical results and it can be used in further simulations.

CHAPTER 4

NUMERICAL INVESTIGATION OF ACOUSTOPHORESIS WITHOUT ANALYTICAL RESTRICTIONS

4.1 Particle Trajectories

In this chapter, the 2D trajectory method of combination of acoustic and hydrodynamic parts is used to obtain particle trajectories inside a closed cavity. 2D cartesian acoustic COMSOL model is integrated into a 2D BEM based Matlab code that solves Stokes equation for given particle and channel configuration using boundary element method. The BEM based code is developped by Dr. Barbaros Çetin's team and used in their previous works [46] [47].The acoustic COMSOL model, combined with this BEM-based code enables us to simulate particles' movements inside a microfluidic channel while taking both acoustic and hydrodynamic interactions into account. Program flow for the 2D integrated trajectory method is given in Figure 4-1below.

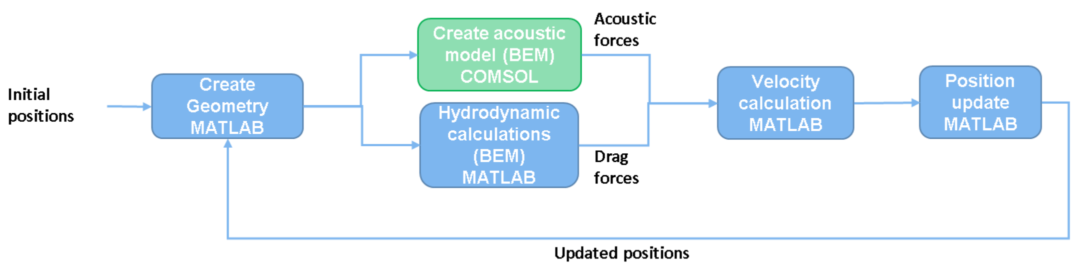

Figure 4-1 Program flow for trajectory calculation with Method 1

Another method called Method 2 is also created by the integration of acoustic and hydrodynamic models designed and tested in the scope of this thesis. A MATLAB code provides communication between the acoustic and hydrodynamic models.

Similar to Method 1, the initial particle-channel configuration is defined in MATLAB, and velocity calculation is again done in MATLAB (Figure 4-2). Unlike Method 1, the second method uses hydrodynamic FEM models explained in sections 3.5.1 and 3.5.2 for the resistance matrix. Depending on which hydrodynamic FEM model is used, this method can ignore or include hydrodynamic interactions.

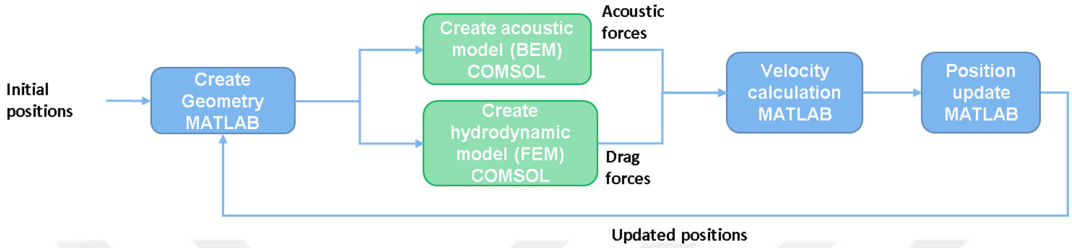

Figure 4-2 Program flow for trajectory calculation with Method 2

A simple case of 2 circular particles of 5 um radius in an acoustic field is simulated using both Method 1, and Method 2 with both acoustic and hydrodynamic interactions are included. Particles are modeled as polystyrene, and they are placed in a closed cavity of 0.4 mm width and 0.3 mm height. Acoustic standing half-wave in y-direction is created in the cavity at 2.4 MHz frequency. Particle initial positions are given in Table 4-1. Distance in x-direction and y-direction between particles is 20 µm and 10 µm, respectively.

Trajectories are simulated for 5 seconds with a time step of 0.25 s. Initial positions and the trajectories obtained with Method 2 are given in Figure 4-3. It should be noted that x=0 and y=0 lines represent channel walls with sound-hard boundaries in acoustical sense and no-slip boundaries in hydrodynamic sense. The same case is also simulated using Method 1, and the resulting trajectories obtained from both methods are compared in Figure 4-4.

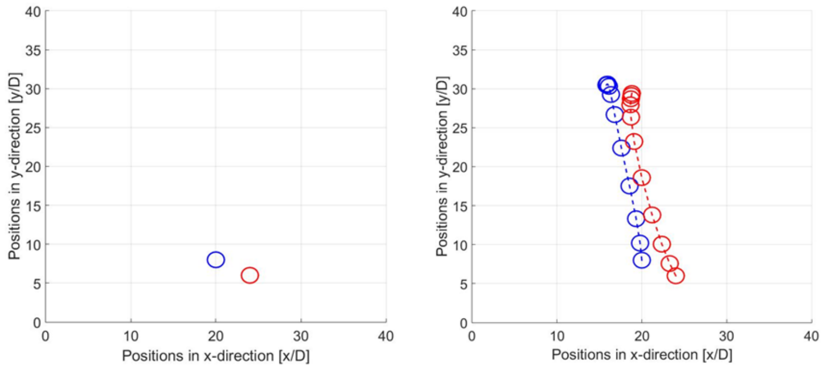

Figure 4-3 Trajectories of circular particles obtained from Method 2

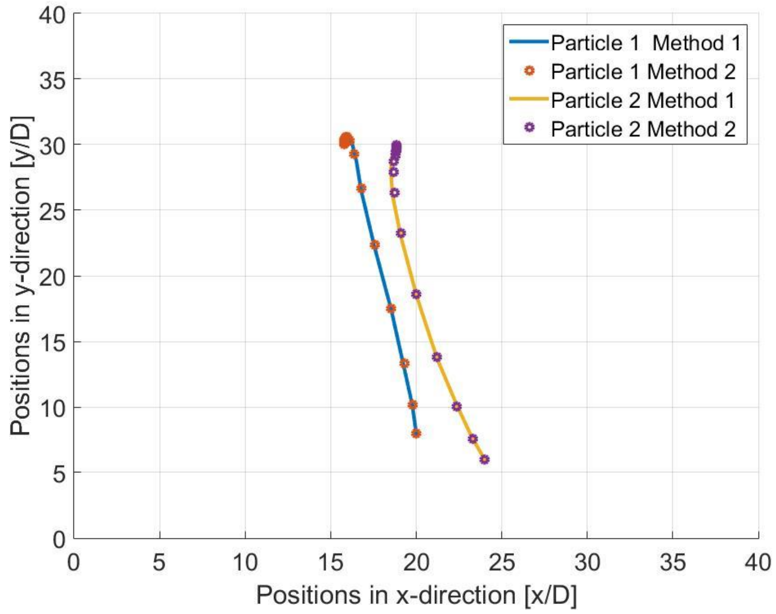

Figure 4-4 Comparison of trajectories obtained from two methods

It is seen from the comparison that Method 2 developed for this study is in good agreement with Method 1. The maximum difference between horizontal and vertical position values obtained from two methods at any time step is less than 2% for vertical positions and 1% for horizontal positions. A maximum of 2% vertical position difference occurs at intermediate steps and vanishes as particles approach the pressure nodal line while horizontal difference at any time step remains and results in a cumulative error at next time steps. The difference between final positions at the end of 5-second-simulation is less than 0.015% in the vertical direction and less than 0.98% for the horizontal direction.

Table 4-1 Initial and final positions

Particle	**Initial position (x,y)**	**Final Position Method 1**	**Final Position Method 2**
Particle 1	(0.1000, 0.0400) mm	(0.0798, 0.1501) mm	(0.0790, 0.1501) mm
Particle 2	(0.1200, 0.0300) mm	(0.0934, 0.1499) mm	(0.0942, 0.1499) mm

4.2 Effect of Walls

Primary acoustic radiation force is an effect of scattering of the incident acoustic wave from the particle surface. In case of the close proximity of other surfaces, such as neighboring particles or walls, re-scattering occurs between surfaces and leads to the secondary acoustic radiation force on the particle. Secondary forces are highly dependent on the distance between surfaces.

The effect of walls is shown with a case of a single particle near a rigid wall. For the different values of particle-wall distance d, total acoustic radiation force is calculated by integration over particle boundary. Simulation results are compared to the analytical results, which considers only primary acoustic radiation force. Comparison of analytical and numerical results for different d/D ratios can be seen in Figure 4-5. Numerically calculated force values are normalized by dividing into the analytical values. And the distance is also non-dimensionalized by using d/D where D is the particle diameter.

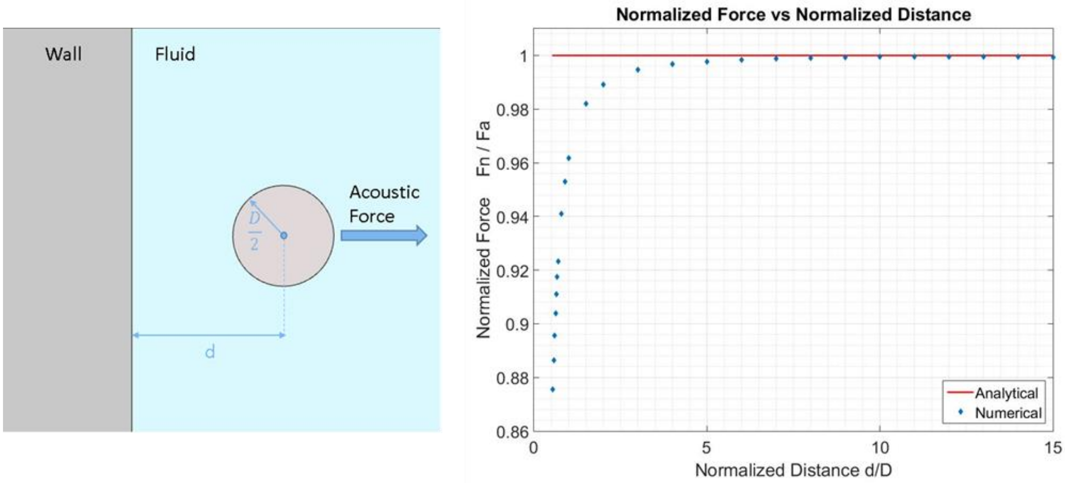

Figure 4-5 Force on particle located near a rigid wall

It can be observed that the numerical result diverges from the analytical one as the distance between the particle center and wall gets smaller. It is clear that the difference between numerical and analytical results indicates the secondary acoustic radiation force due to re-scattering effects. At distances, less than one diameter, numerically evaluated total acoustic force corresponds to less than 90% of the primary acoustic radiation force which was obtained from the analytical formula. Therefore it indicates secondary acoustic radiation force in the opposite direction. When the particle is placed more than six diameters away from the wall, secondary effects almost vanish, and starting from this point, numerical and analytical results come to good agreement, showing that after six diameter distance from the wall, it is safe to assume an isolated particle.

Having seen the effect of wall on the acoustic force, trajectory of particle near a rigid wall is simulated using Method 1 with combination of acoustic and hydrodynamic interactions between the particle and wall. To observe the effects, trajectory is also calculated using analytical formulations for both acoustic and hydrodynamic physics. The analytical calculation, as mentioned before, considers the particle is acoustically and hydrodynamically isolated. Therefore includes no interaction effects.

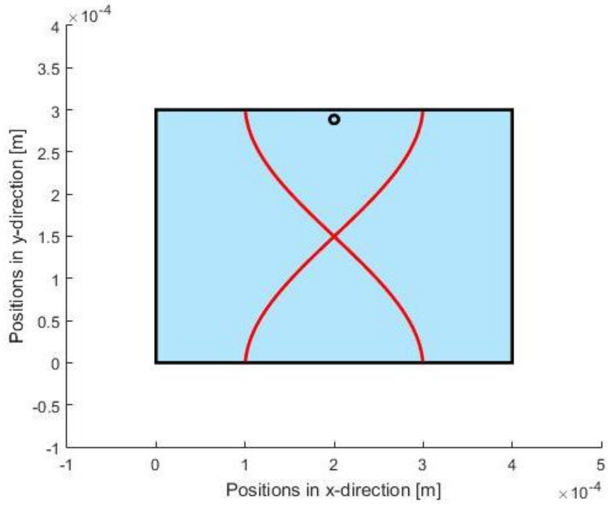

Figure 4-6 Initial position of the particle in the acoustic field

Trajectory of a particle with 5 μm of radius inside an 0.4 mm by 0.3 mm closed cavity is simulated. Particle starting position is defined as 6 μm from the upper horizontal wall (Figure 4-6). Under the influence of the acoustic standing half-wave in the y-direction, particle moves towards the pressure nodal line at y=0.15mm. The change of the vertical position of the particle obtained from Method 1 can be seen in Figure 4-7. The analytical method consists of Gorkov's formulation for acoustic part and Lamb's formulation for the hydrodynamic part. Analytical method predicts that the particle reaches the nodal line in 2 seconds while the numerical result shows that, with the acoustic and hydrodynamic interactions are included, it takes 8 seconds to reach the nodal line.

This result shows that analytical methods, ignoring the wall effect, fail to give a realistic scheme for the acoustophoretic separation phenomena. It can be predicted that, with the existence of the bulk fluid flow inside the channel, the particle would not be able to reach the pressure node in the limited time of its exposure to the acoustic field, contrary to the analytical results.

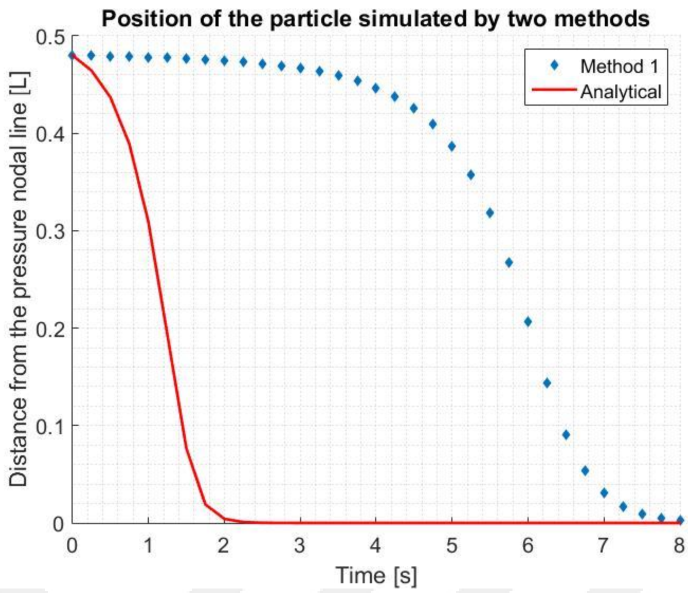

Figure 4-7 Position of the particle in the acoustic field in a channel of width L

4.3 Effect of Particle Shape

One of the main aspects that conventional methods lack is the object geometry. Although some studies provide analytical formulations for non-spherical shapes like spheroids and cylinders, they have some limitations. It is known that Marston's analytical approximation for spheroids is rather accurate for the eccentricities smaller than 1. For more complex geometries, analytical evaluation of the wave scattering from the object surface becomes much more difficult, which directs us to the numerical methods.

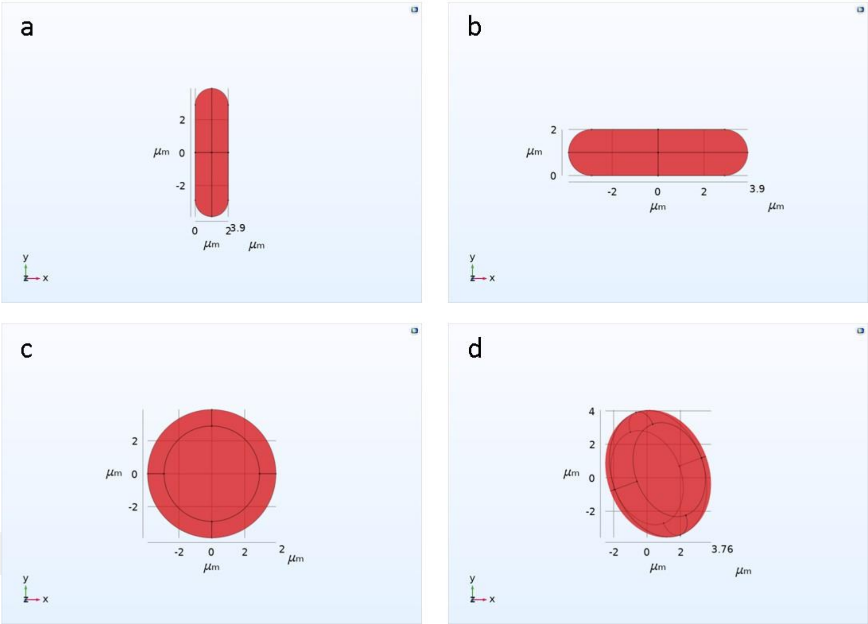

Figure 4-8 RBC symmetry axis is on: x-axis (a), y-axis (b), z-axis (c), θ=45˚,φ=20˚ in spherical coordinates (d)

A red blood cell (RBC) geometry is modeled in COMSOL (Figure 4-8) in the water domain. An acoustic field of 2 MHz is applied on the fluid domain by a plane standing wave of 100 kPa at x-direction, and the resulting acoustic force on the cell is obtained from surface integration. The acoustic force that acts on the RBC is calculated for different angular positions of the cell where its symmetry axis lies on different axes. Results are normalized by the acoustic force calculated in the first case where RBC axis is aligned with the x-axis. The torque value of the second case where RBC axis is on the y-axis is used for normalization of torque values in all cases. Force components in y and z directions are also calculated; however, they are smaller than the x-force by up to 1000 fold, therefore not given in the table. The remaining torque values are eliminated due to the same reason. Results are given in Table 4-2. According to the table, shape, and orientation has no significant effect on the acoustic force with the cell material properties, which are close to the surrounding fluid. However, due to the shape and orientation, acoustic radiation torque arises on particle which is not in a rotational equilibrium position according to the wave. No such effect is observed for the equivalent sphere with the same volume as RBC, due to its shape and for the RBC whose axis is on wave direction.

Table 4-2 Acoustic force at each cell position

RBC symmetry axis	**Normalized Acoustic Radiation Force**	**Normalized Acoustic Radiation Torque**
x	1.0000	0
y	0.9688	Tz=1.0000
z	0.9681	Ty=-1.0113
θ=45˚,φ=20˚ in spherical coordiantes	0.9834	Ty=-1.5629 Tz=0.5335
Equivalent Sphere	0.9747	0

Force acting on the RBC depends on the orientation of the cell according to the wave direction. Even though the force in x-direction is not significantly different from the equivalent sphere approximation, the resulting torque acting on the particle is likely to affect the trajectory. This effect is shown with the trajectories of a needle-like elliptic particle and an equivalent circle in 2D simulations. Single elliptic and circular particles are placed in the same position in a closed cavity, one by one. The cavity is 0.4 mm by 0.3 mm, and there is an acoustic field in vertical direction at 2.4 MHz. Method 1 is used for the study. Trajectories of the particles are obtained as given in Figure 4-9.

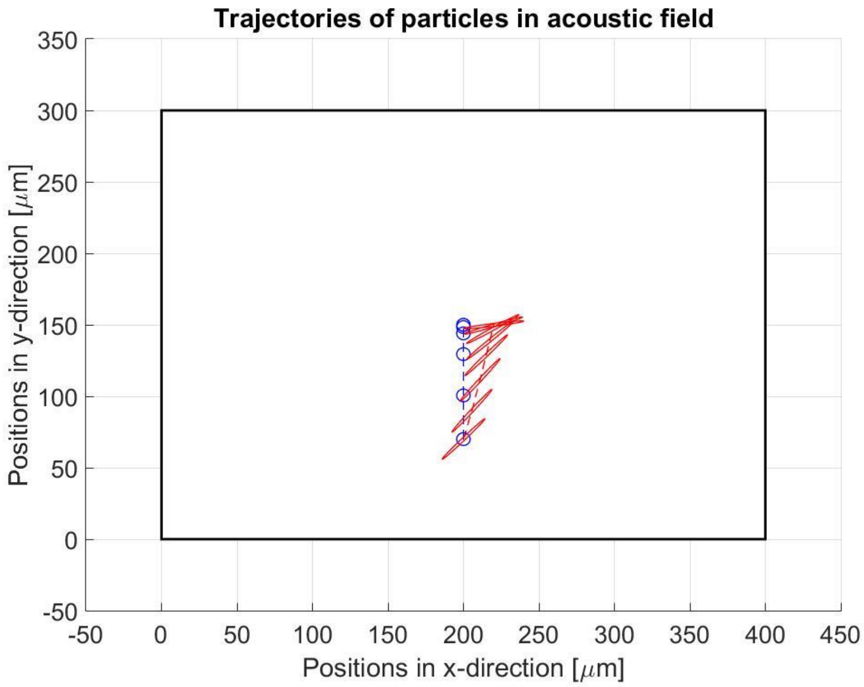

Figure 4-9 Trajectories of single circular and single elliptical particles plotted together

Results show that, elliptical particle's trajectory diverges from a straight line due to its shape. The most prominent effect is that, although the acoustic force is in the vertical direction, elliptic particle has a velocity in the horizontal axis, too while no such effect is observed for circular particle. It is the result of the hydrodynamic effect. As a second step, trajectories of the elliptical particles at different starting angular positions (0˚,45˚,90˚,135˚) are simulated in the same way. (Figure 4-10).

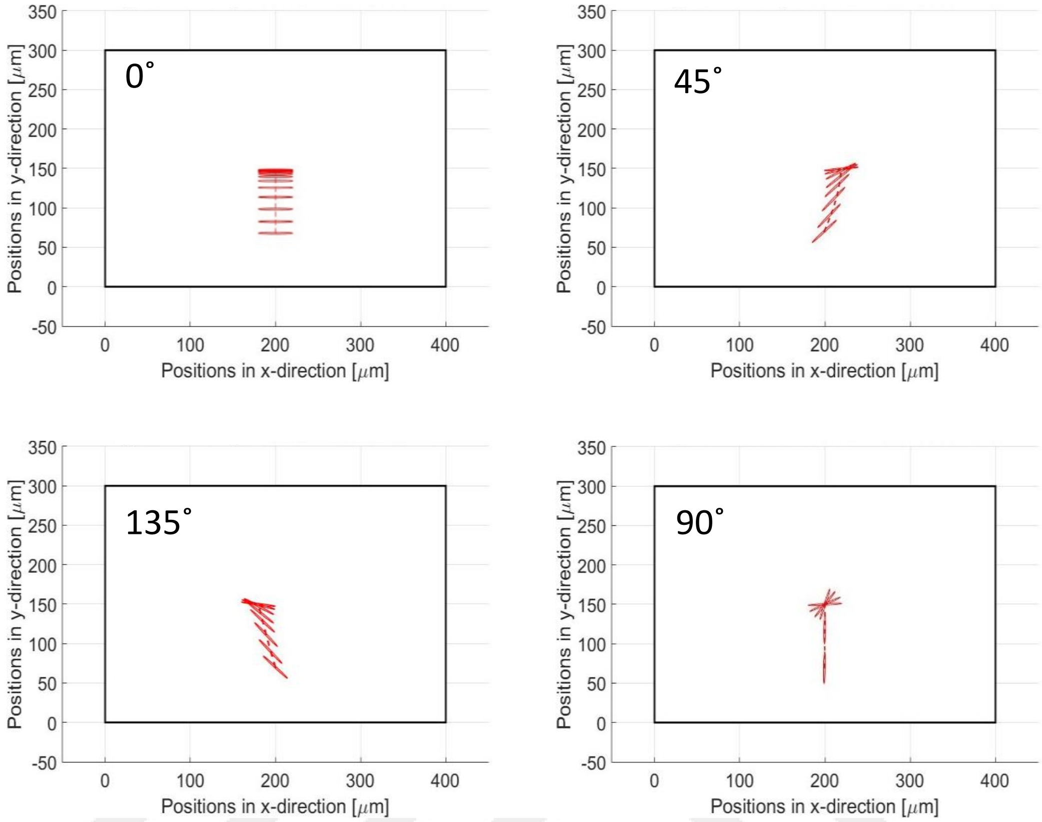

Figure 4-10 Trajectories of elliptical particles with different starting angular positions

It is also seen that the trajectory of the elliptical particle highly depends on the starting angular position of the particle. While the particle at 0˚ does not rotate, the particles at 45˚ and 135˚ degrees rotate at the same time as moving towards the nodal line. On the other hand, the particle at 90˚ does not rotate at first, and then it aligns itself after reaching the nodal line. Eventually, in all cases, the ellipse's major axis becomes perpendicular to the wave direction at the equilibrium position.

Looking at the forces and velocities acting on the particle at the initial position, one can observe that acoustic radiation force in wave direction does not change significantly between ellipses and the circle. However, for the 45˚and 135˚ positions, it appears that there is an acoustic radiation torque acts on a particle, in addition to the force. This acoustic effect combining with the hydrodynamic one shows that among all the cases, circle has the maximum translational velocity while the ellipse at 0˚ has the minimum, and both have almost no rotational velocity. Normalized force, torque, and velocity values are given in Table 4-3. Normalization was performed for force and translational velocity values by dividing them by the force and velocity of the circular particle. A similar procedure was applied to the torque and rotational velocities by dividing them to the corresponding values of the elliptic particle at 45˚.

Table 4-3 Force and torque acting on particles at the initial position and resulting velocities

Particle	**Normalized force in y**	**Normalized torque**	**Normalized velocity in y**	**Normalized rotational velocity**
Circular	1.0000	0	1.0000	0
Elliptic, 0˚	1.0040	0	0.4766	0
Elliptic, 45˚	0.9911	1.0000	0.6482	1.0000
Elliptic, 90˚	0.9783	0.0350	0.8099	0.0357
Elliptic, 135˚	0.9910	-1.0000	0.6482	-1.0000

Vertical positions in each case are plotted together in Figure 4-11. Having the maximum velocity among all, the circular particle becomes the first one to reach the nodal line in 2.3 s, followed by ellipse at 90˚. It takes 4 seconds for ellipses at 45˚ and 135˚, and lastly arrives the ellipse at 0˚.

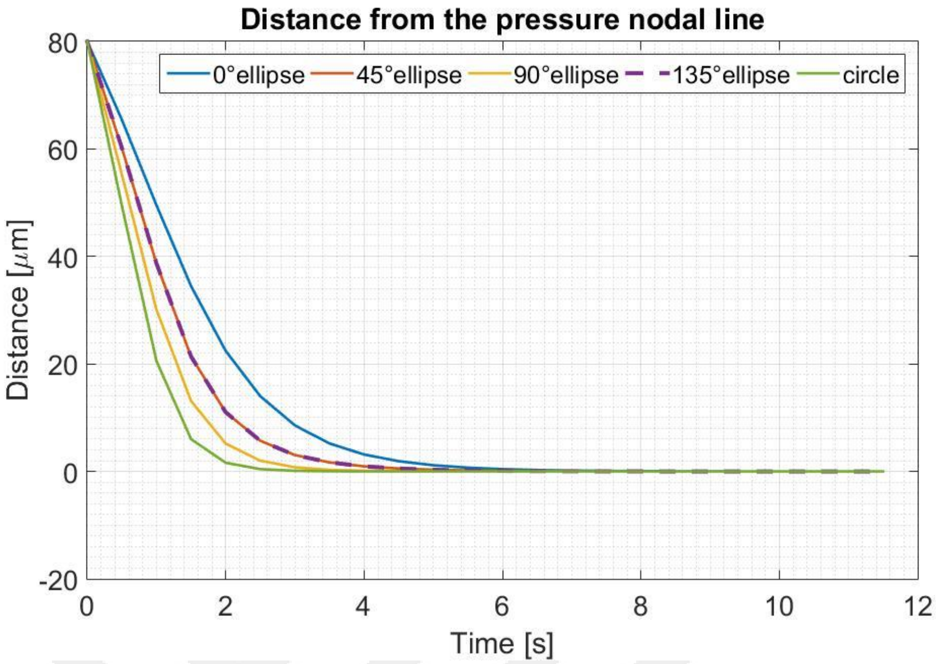

Figure 4-11 Vertical positions of the particles changing with time

4.4 Effect of Particle Concentration

Concentration is another factor that affects acoustic radiation force on particles. In this section, the effect of neighboring particles is analyzed. The existence of other objects around the main object causes re-scattering of acoustic wave from neighboring particle surfaces; therefore, secondary acoustic radiation force on the main particle arises. Divergence from the analytical formulation due to the particle concentration was shown in the following case.

A block geometry is created with an acoustic field inside of it. For the first configuration, a single particle is placed inside the block, which corresponds to 0.01% volume of the total block volume. Model is solved using FE method, and the force on the particle is recorded. For the second case, the number of particles is kept the same; however, a smaller block is defined. And for the third and the fourth cases, the block size was decreased further while the number of particles is increased to 10 and 18, respectively. Configuration geometries are given in Figure 4-12. Acoustic forces acting on the particles in each configuration are compared to the analytical formulation, which considers each particle as isolated. Walls are modeled as sound-hard boundaries; therefore scattering from the walls is also considered.

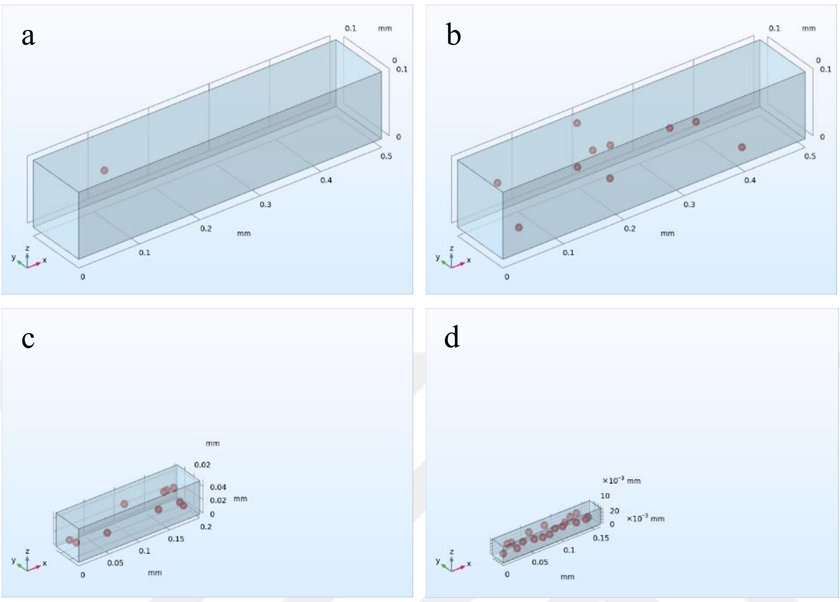

Figure 4-12Configuration Geometries: Configuration 1 (a), Configuration 2 (b), Configuration 3 (c), Configuration 4 (d)

Forces acting on each particle in each configuration are calculated numerically and compared to the analytical result for an isolated particle, which gives primary acoustic radiation force. Table 4-4 shows how the total acoustic force on particles differs from the primary acoustic radiation force as the particle concentration inside the box increases. For the first configuration, almost no secondary acoustic force ascends. As the block size is reduced and the number of particles is increased, total acoustic radiation force differs by up to 6% due to the secondary acoustic radiation force.

Table 4-4 Model parameters and results/Concentration

No	**Channel Dimensions [mm x mm x mm]**	**Number of Particles**	**Volume Concentration (%)**	**Divergence from analytical solution (%)**
1	0.5x0.1x0.1	1	0.01	0.11
2	0.5x0.1x0.1	10	0.10	0.80
3	0.2x0.05x0.05	10	1.05	1.38
4	0.16x0.024x0.024	18	10.22	6.08

To investigate the concentration effect on particle trajectories, a two-dimensional case of 32 circular particles inside a closed cavity is modeled. Particles are exposed to an acoustic half-wave in the vertical direction. Method 1 is used to include interactions in both acoustic and hydrodynamic parts. They are distributed to two sides of the channel. Distance between particles in each side of the cavity varies in a range of 8 to 15 diameters.

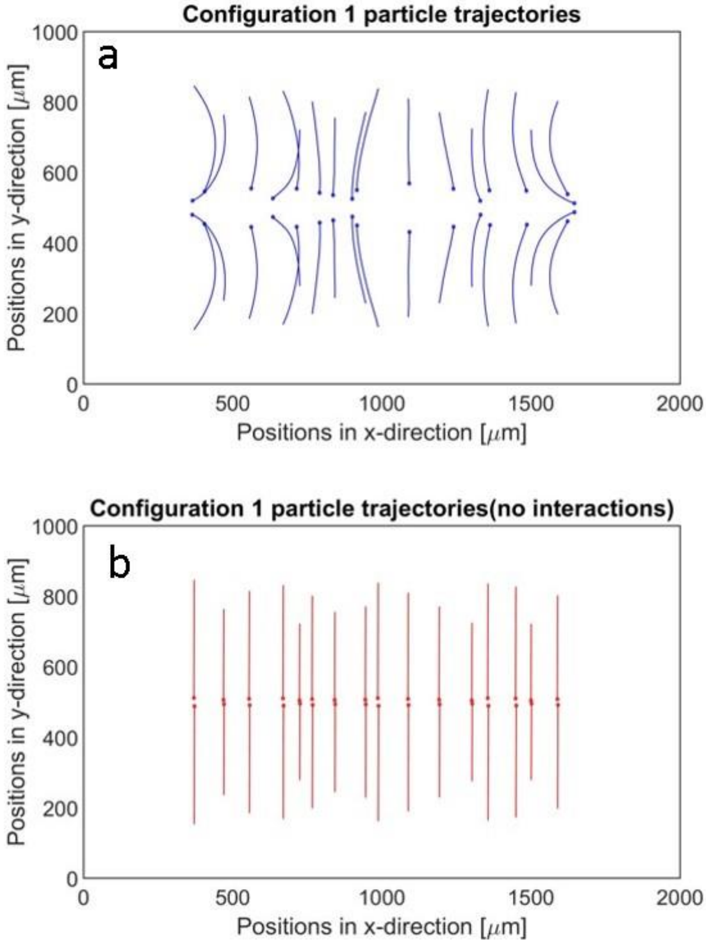

Figure 4-13 Trajectories of particles for Configuration 1: with all interactions (a), without interactions (b)

Trajectories given in Figure 4-13 (a) are calculated, accounting for both acoustic and hydrodynamic interactions. Later, the same configuration is studied with Method 2 while considering only acoustic interactions and with Method 1 while the analytical formulation is used for the acoustic part; hence this study only considers hydrodynamic interactions. And the last study for this configuration was performed accounting for no interactions. These studies show that hydrodynamic interactions for this particle configuration are the dominant effect that cause the trajectory paths to diverge from straight lines towards the nodal line as it was predicted by analytical methods.

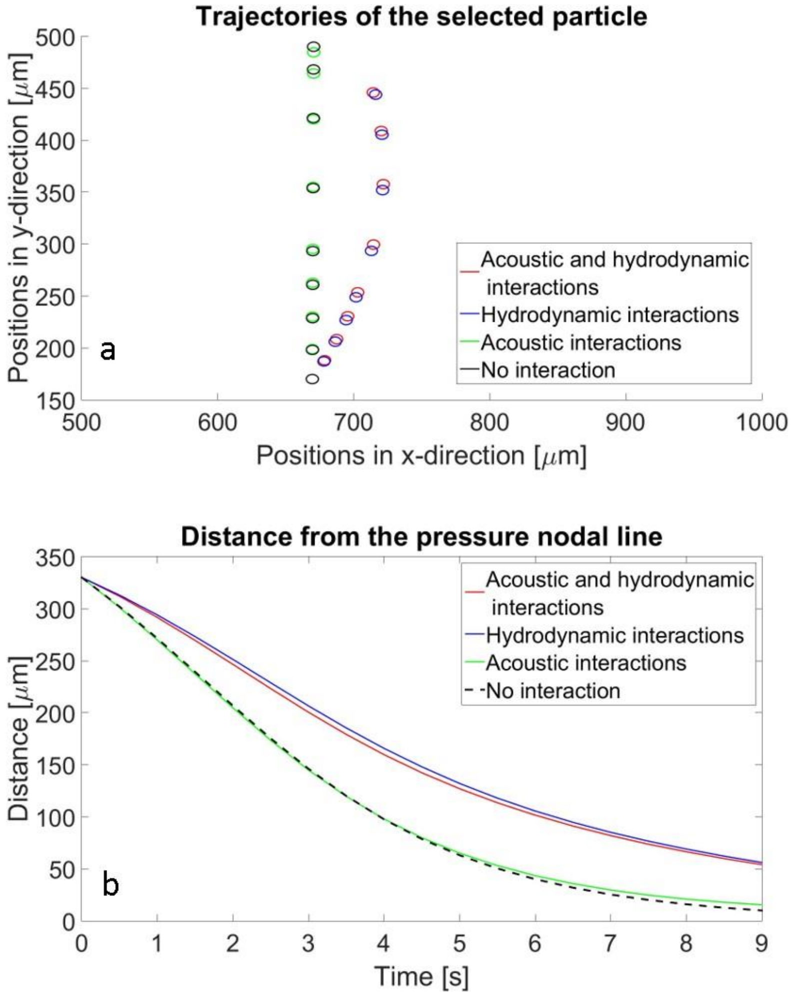

Figure 4-14 Trajectory of the selected particle obtained from different simulations (a), particle's distance from the nodal line

One particle is selected from the simulations of Configuration 1, and its trajectories, obtained from four different simulations, are plotted together. Figure 4-14 shows that acoustic interactions in 9-second simulations have a smaller effect than the hydrodynamic one. Particle's curvy trajectory results from hydrodynamic interactions, while acoustic interactions lead to the small difference in y-position. It is also possible that interactions increase as particles gather around the pressure nodal line; therefore, particles could not reach the nodal line when all interactions are included, unlike the 'No interactions' case.

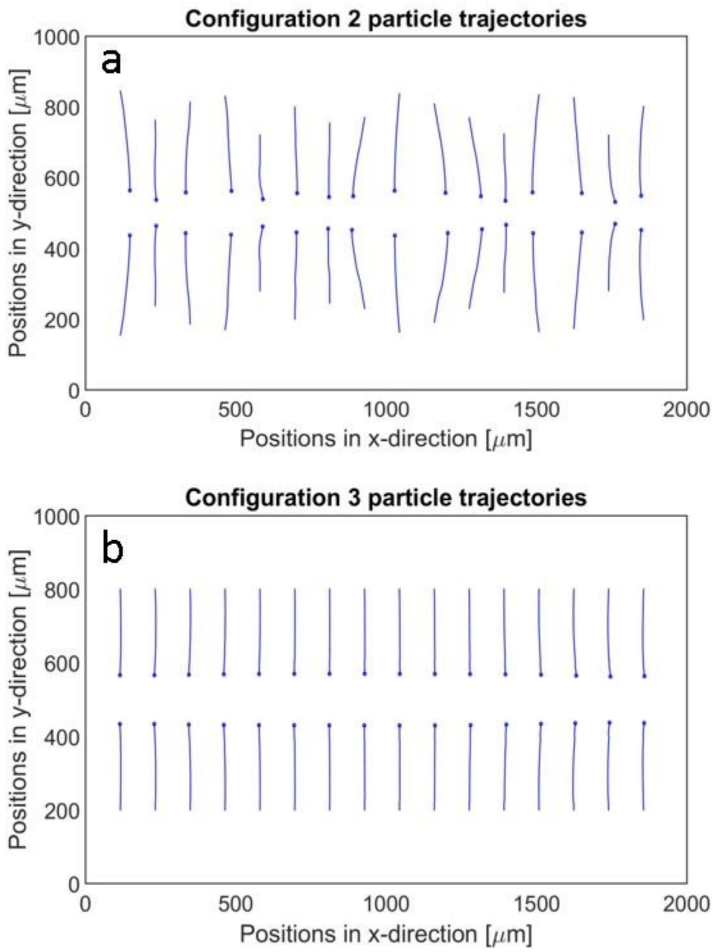

Figure 4-15 Resulting trajectories: Configuration 2 (a), Configuration 3 (b)

The second configuration is designed by extending the horizontal distance between particles to more than ten diameters while keeping the same vertical positions. It is solved by using Method 1. As a result, hydrodynamic interactions decreased considerably, and particle paths become less curvy. However, there is still an interaction visible in Figure 4-15(a) despite the increased inter-particle distance. To investigate this, a third configuration is simulated with Method 1 where vertical positions of particles are all set to the same value for each side of the nodal line; therefore, all particles have the same distance from the horizontal walls. Positions in the x-direction are kept as the same in Configuration 2.

Despite the fact that inter-particle distances are less than the ones in Configuration 2, particle interactions are mostly eliminated in the third configuration. Particles follow almost straight lines towards the nodal line (Figure 4-15(b)). Difference between Configurations 2 and 3 shows the effect of inter-particle distance in the force direction. An observation is that particles approach to other particles ahead of them in their path to the nodal line. When all particles have the same vertical distance to the nodal line, no such effect is observed.

In order to add the shape effect to the concentration study, Configuration 1 is used again, changing half of the particles with the ellipses of the same area. The ratio of the radii in major and minor axes is 20. Resulting trajectories are given in Figure 4-16 (a). Difference between Figure 4-13(a) and Figure 4-16(a) is due to the existence of elliptical shape. Consider the same particle whose trajectories are shown in Figure 4-14(a). It is selected again and shown in the green circle in Figure 4-16(a). This time, its movements in the pure-circular suspension and mixed suspension where half of the particles are elliptic are compared in Figure 4-16(b). In both cases, the selected particle is a circular one, and all particles have the same initial positions under the same acoustic field. Neighboring an elliptical particle instead of a circular particle in the same position causes more than a 6-diameter difference in final x-position.

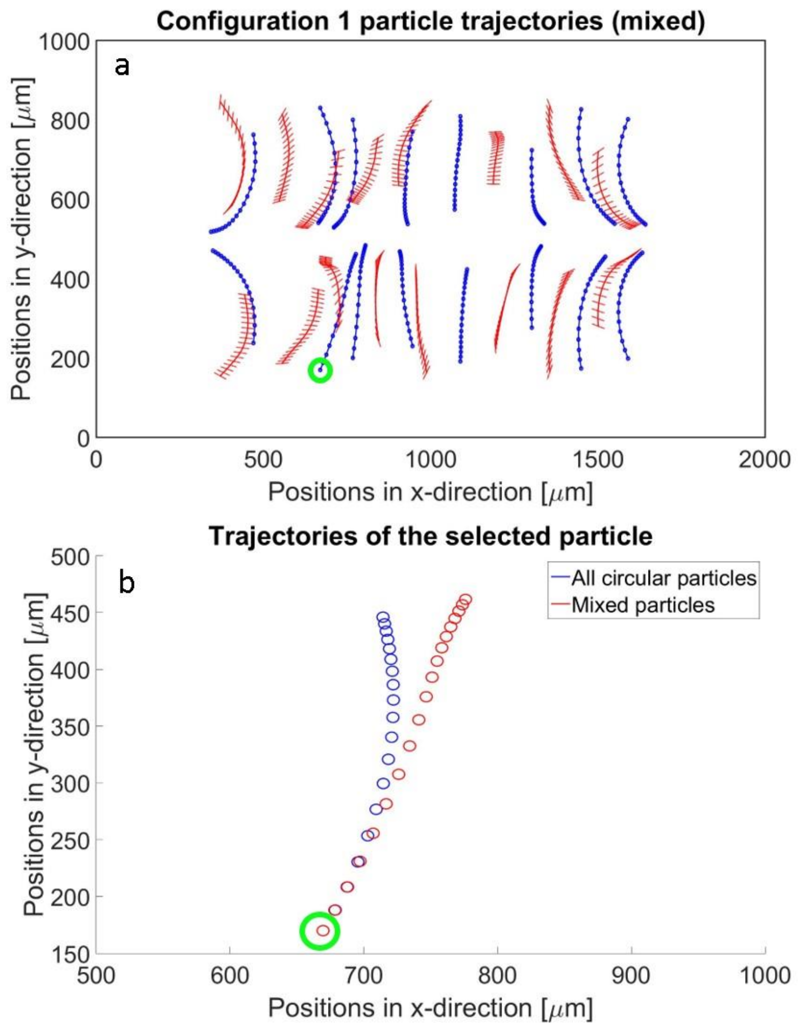

Figure 4-16 Trajectories of mixed elliptic-circular particles in Configuration 1 (a), selected particle's trajectories when it is in all-circular and mixed suspensions (b)

In this chapter, different parameters affecting trajectories of particles inside an acoustofluidic chamber are investigated. The proposed numerical tool consisting of acoustic and hydrodynamic parts is used to simulate particle trajectories inside the chamber. Wall, shape and concentration effects on acoustic radiation force is first investigated, and then their effects are visualized at trajectories. Combined effects in the both acoustic and hydrodynamic parts regarding to each factor are seen on the particle trajectories.

CHAPTER 5

DEVICE LEVEL SIMULATIONS WITH NUMERICAL ACOUSTOPHORETIC FORCE CALCULATIONS

5.1 Device Model

After investigating the effect of many parameters in the previous chapter, the concept of acoustophoresis with these parameters is extended to the device level. A simple acrylic microfluidic device model with a piezo element as an actuator is modeled in COMSOL. This acoustic model includes a piezoelectric material integrated to the chip material. With an electric potential input, the vibration of piezoelectric material causes acrylic chip to vibrate, which eventually creates the acoustic field inside the channel which is modelled as a fluid domain. In this model, COMSOL software is used where piezoelectric transducer is modeled with solid mechanics module with electrostatics coupling, chip material is modeled as an acoustic domain with attenuation and FEM is used for both. Fluid and particle domains are considered as linear elastic acoustic domains. FEM is again used inside the particle domains and BEM is used for the fluid domain. Therefore, an acrylic microfluidic device with a piezoelectric actuator is modeled in 2D to obtain the acoustic force on compressible particles inside the fluid with BEM and FEM approaches coupled. Acoustic COMSOL model is built with an excitation frequency of 900 kHz on the piezoelectric actuator (PZT-4). 20V electric potential difference is supplied to the PZT-4 material, which leads to the displacement in the first part of Figure 5-1 (a). As a result of the displacement, an acoustic field is created in the acrylic and fluid domains (Figure 5-1(b) and Figure 5-1(c)).

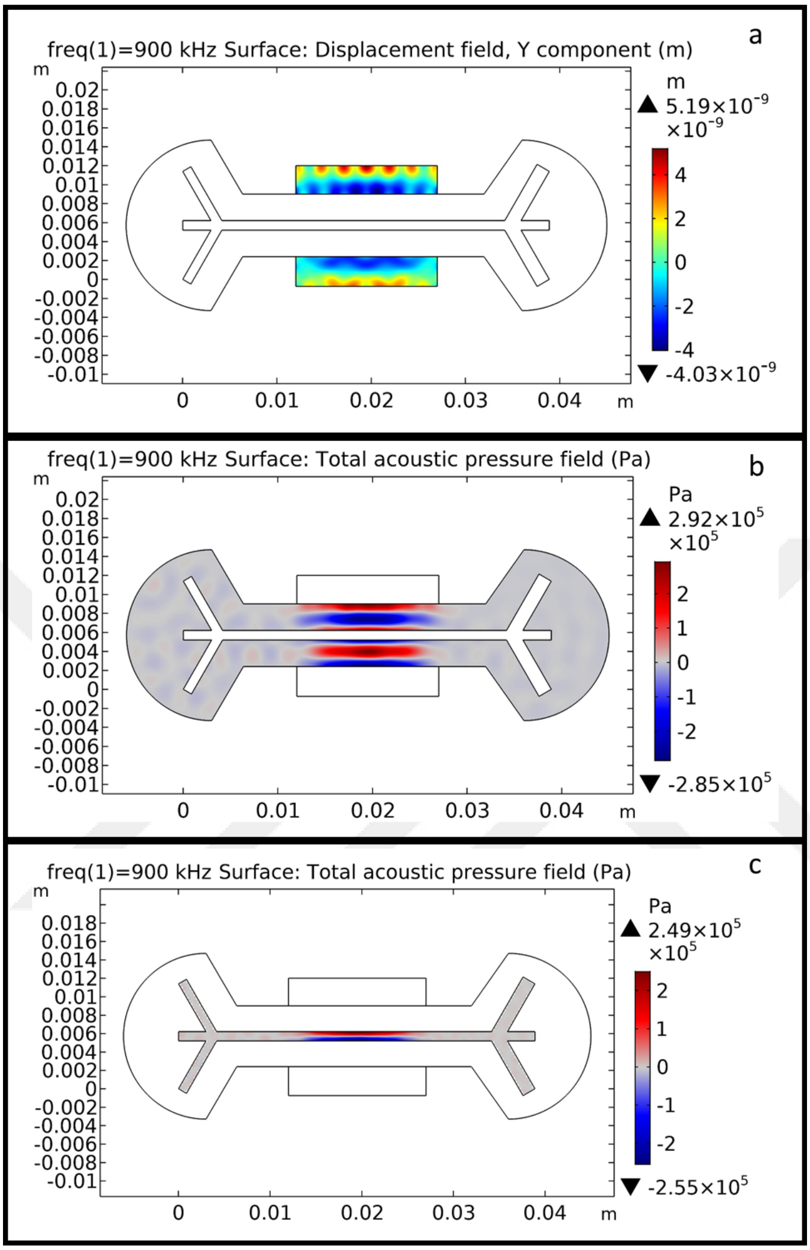

Figure 5-1 2D Acoustic device simulation: Surface displacement field in piezoelectric material (a), Resulting acoustic field in the chip material(b), Acoustic field inside fluid domain (c)

To calculate the trajectories of particles inside the channel, the above-mentioned COMSOL model is again integrated to the BEM-based MATLAB code for hydrodynamic calculations. The integrated method is the device-level version of Method 1 explained in Chapter 4. Therefore, this method simulates particles' movements inside the microfluidic channel with a bulk fluid flow and takes account for both acoustic and hydrodynamic interactions, allowing simulation of non-spherical particles.

5.2 Simulation Case

This simulation case includes 10 particles, half of which are elliptical and the other half is circular. All particles have the same area and material properties representing polystyrene. Particles enter the channel from one of the side inlets only. A bulk fluid flow is existent in main inlet and side inlets at average flow velocities of 3 mm/s and 0.5 mm/s, respectively. The main channel has 1mm of width and is nearly 39 mm in length. Side outlets have 1.6 mm width. 12 V electric potential difference is supplied to the piezoelectric material, which leads to the acoustic field of 143 kPa magnitude in the channel. This study aims to examine the difference in acoustic manipulation of particles due to particle shape. In literaure, we have found no device level simulations with non-spherical particles. Trajectories of particles are obtained using device-level simulation with Method 1, including acoustic and hydrodynamic interactions. Initial positions of particles are shown in Figure 5-2.

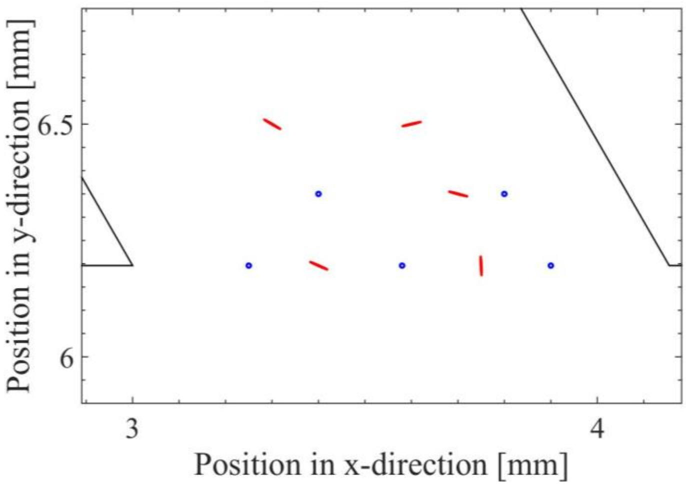

Figure 5-2 Initial positions of the particles

Simulation result of a mixed particle suspension for 9.6 seconds is given below. Red dotted lines represent the elliptical particle trajectories while the blue dotted lines represent the circular particle trajectories. Particle movements in inlet, in the middle of the channel and the outlet are given in Figure 5-3.

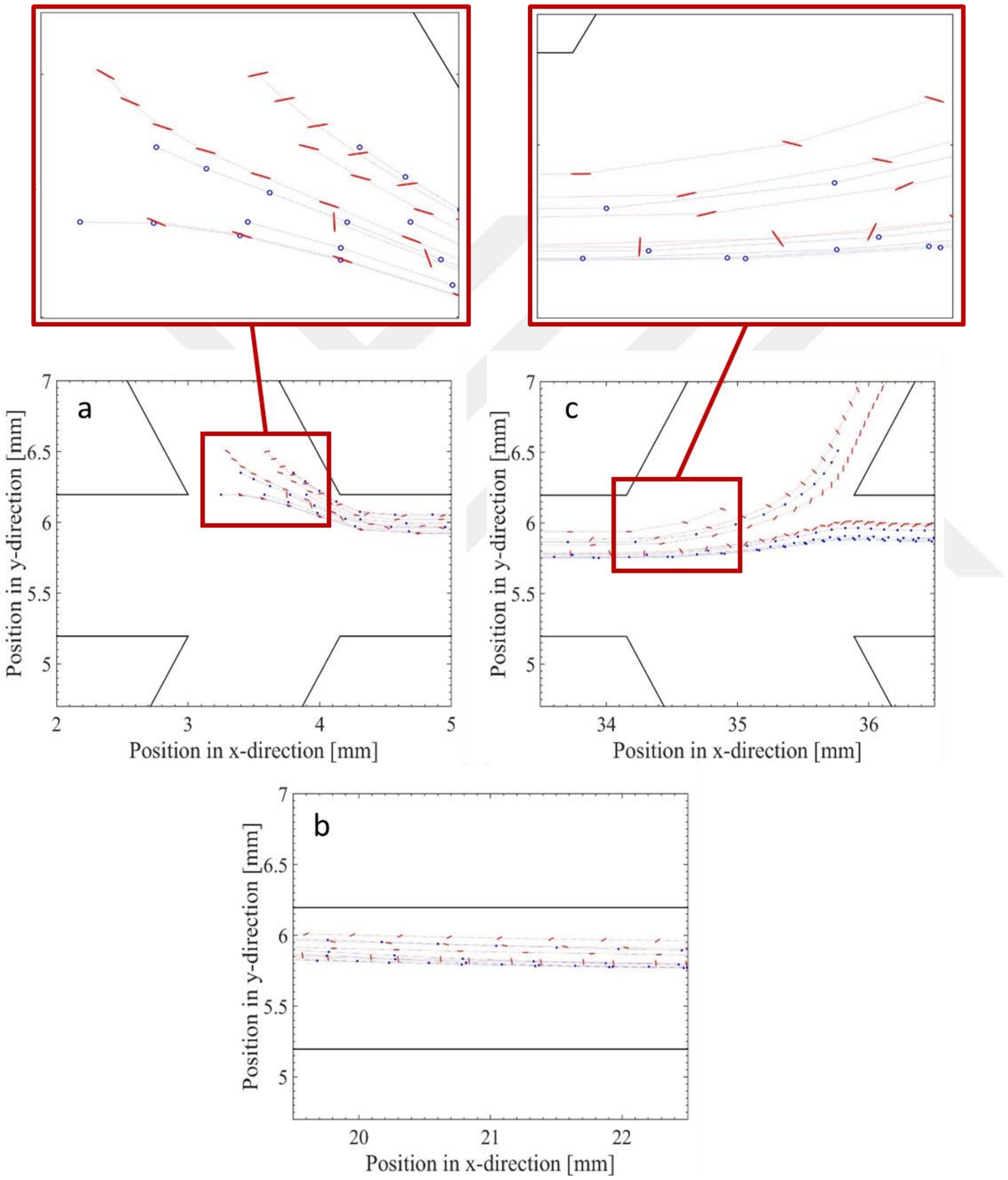

Figure 5-3 Mixed particle trajectories in the inlet (a), in the middle (b), and in the outlet (c)

Mixed particle simulation shows that elliptical particles that are initially placed at arbitrary positions rotate around their center while they move through the channel with the fluid flow. Suppose the angle between the ellipse major axis and the horizontal x axis is considered. In that case, it will be seen that the ellipses with smaller angles could not reach the channel centerline as fast as the circles, since the vertical velocity of the ellipses aligned in the horizontal axis is smaller than circles and the other ellipses whose major axis is perpendicular to the wave direction as it was discussed in Chapter 4. As a result, three of the elliptical particles and a circular particle leaves the channel from the side outlet while the other two ellipses with higher angle values (c) leaves from the main outlet along with other circular particles since these ellipses already reached the pressure nodal line before. It shows that the acoustic manipulation of the elliptical particles highly depends on the particles' angular position when they are exposed to the acoustic field inside the channel.

Same case is also simulated with equivalent circular particles consisting of 10 circles with the same area. Particle initial positions, flow velocities, voltage input and the simulation time are kept as the same. Result of this simulation is given in Figure 5-4. Each dotted line shows a particle trajectory and the particle position at each time step are marked on the lines. Three circular particles leave from the side outlet. However, when compared to the mixed-particle simulation, most of the particles in the all-circular case are focused on a narrower band than in the mixed-particle case. This result shows that equivalent sphere approximation may not accurately simulate the acoustophoretic motion or seperation of non-spherical particles. Our simulations show that even with equal area, it is also possible to separate the elliptical andcircular particles of the same material using acoustophoresis with appropriate voltage and outlet flow conditions.

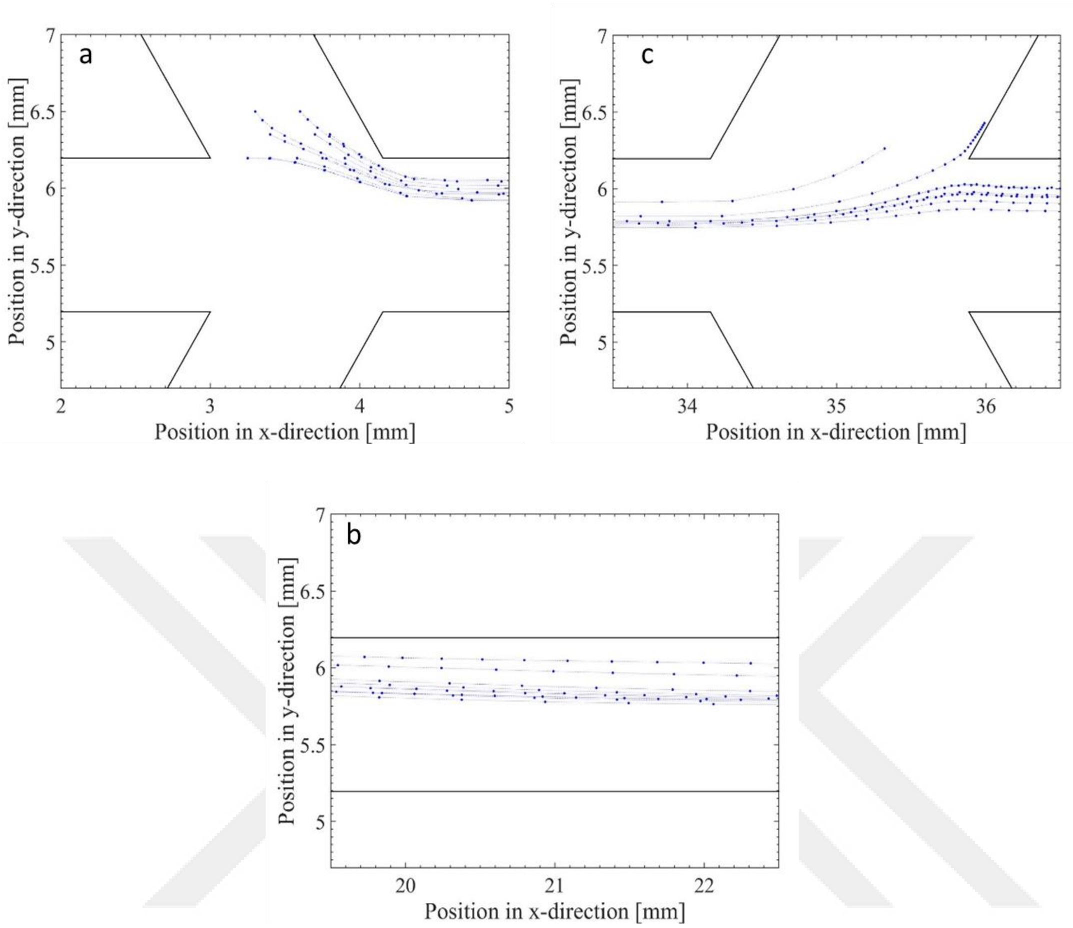

Figure 5-4 Circular particle trajectories in the inlet (a), in the middle (b), and in the outlet (c)

CHAPTER 6

CONCLUSIONS AND RECOMMENDATIONS

Acoustophoresis is a promising tool for manipulating bio-particles inside microfluidic devices due to their gentle manipulation to the cells hence offering high cell viability. Movement of particles inside the device results from the acoustic radiation force exerted on the particle. Acoustic radiation force is obtained from the integration of second-order acoustic pressure over the particle boundary. There are analytical solutions for acoustic radiation force on small, isolated spheres and some non-spherical particles such as cylinders or spheroids with small eccentricity. However, biological samples often appear in non-spherical shapes and high sample concentrations. Also, some biological applications may require manipulation in higher frequencies for more precision and selectivity. Therefore, analytical solutions fail to cover these effects. For the cases outside of the analytical frame, a solution can be obtained by numerical methods. Numerical methods provide an opportunity to obtain acoustic radiation force on arbitrarily-shaped particles and the acoustic interactions between particle and its surroundings which are not possible with the analytical methods.

In this thesis, BEM and FEM methods are used to simulate acoustic particle manipulations with considering other shape and concentration-related effects. In order to calculate acoustic radiation force numerically, COMSOL Multiphysics software is used. Three simple cases, which have analytical solutions, are simulated using the COMSOL models to verify the proposed model against the analytical solutions. 3D acoustic models are created using BEM, FEM, and coupled BEM-FEM approaches. Because of the computational burden of 3D models, 2D axisymmetric models are also tested since it is possible to extrapolate the integration results from

2D to 3D in this model. Lastly, the 2D cartesian model is created to verify the simulation models against 2D approximation of Gorkov’s formula. Proposed simulation models show good agreement with the analytical solutions, especially for 3D and 2D cartesian models with errors less than 0.2%. In addition to the acoustic simulation model, a FEM-based hydrodynamic model is aso created to calculate viscous drag force on arbitrarily-shaped particles. This model is verified against the analytical solutions for sphere, spheroid, and cylinder with unit length. Numerical results do not differ from the analytical ones more than 0.7%. Therefore numerical tools can reliably be used to calculate acoustic radiation force and viscous drag force to obtain particle trajectories.

To simulate the particle movements under acoustophoretic force, two simulation methods are proposed. First method is created by integrating the acoustic BEM-based COMSOL model with a BEM-based MATLAB code, while the second method uses the FEM-based COMSOL model, verified in Chapter 3 before, for hydrodynamic calculations. Both methods use the same acoustic model which takes acoustic interactions into account. Method 1 includes all hydrodynamic interactions between the particle and the surroundings while it is optional for Method 2. Trajectories of two circular particles are calculated using both methods including both acoustic and hydrodynamic interactions. At the end of 5-second simulations, the final positions of particles have less than 0.015% difference in vertical direction and less than 0.98% difference in horizontal direction.

A channel confinement study is performed to show the wall effect on the acoustic radiation force. A particle is located near a hard-wall in an acoustic field to go beyond the isolated particle assumption. Numerically-calculated total acoustic force on particle is compared to analytical force values. Results show that for distances less than 1 diameter, the secondary acoustic radiation force's effect becomes prominent and reaches almost 10% of the primary force in magnitude. The effect of wall is also shown in particle trajectory. Simulation of the case with Method 1 shows that time required for particle to reach the pressure nodal line is 4 times that the analytical solution suggests.

Effect of particle shape is examined in the RBC case. A red blood cell geometry in 3D is created in an acoustic field at different orientations and resulting force values at each position are compared to the equivalent sphere shape. Results show that for given cell material properties close to the surrounding fluid properties, acoustic force in the wave direction does not differ significantly between RBC shape and equivalent sphere. However, for RBC shape, there appears acoustic radiation torque on particle which is non-existent in equivalent sphere case. Therefore, RBC trajectory is likely to differ from a spherical particle trajectory obtained by analytical methods. The effect of shape on the trajectory is also investigated in 2D case with using Method 1. It is observed that a needle-like elliptical particle has a different trajectory than an equivalent circular particle mainly due to the acoustic torque and the hydrodynamic effects related to the shape. It is also seen that the trajectory of elliptical particle highly depends on the angular position of the ellipse.

Concentration effect on total acoustic force is investigated by gradually increasing the particle concentration in a box. Concentration increase is provided by both increasing the number of particles and decresing the size of the channel where particles are located. As a result, as volume concentration goes from 0.01% to 10%, divergence from the analytical result goes from 0.11% to 6% referring to increasing secondary acoustic force effect. For the concentration effect on particle trajectories, 32 circular particles are located in a closed cavity. Particle trajectories obtained with all interactions is compared to the simulation without interactions. It is observed that there is a significant difference between both results due to the hydrodynamic interactions which seem to be the dominant effect. With all interactions included, particles follow curvy paths towards the nodal line and do not agglomerate on the pressure nodal line unlike the simulation result without interactions suggests. In addition, when a shape effect is added to the concentration effect, it is seen that neighboring particle shape has an impact on the particle's trajectory.

Lastly, a device-level simulation is created with a piezoelectric actuator integrated to it. Manipulation of mixed particle suspension of circular and elliptical particles inside a microfluidic channel is simulated by considering both the acoustic and hydrodynamic interactions. The same case is also simulated with pure-circular suspension with the same particle release positions. It is observed that elliptical particles are focused on a larger band around the channel center compared to the circular particles. Therefore most of the ellipses leave from the side outlet. Ellipses, whose major axis is aligned with the flow direction, could not reach the channel centerline during their time of exposure to the acoustic field. This result is consistent with the findings in Chapter 4 and shows that with proper flow and voltage arrangements, it is possible to separate elliptical and circular particles of the same material and same area.

The methods proposed in this thesis provide a better understanding of acoustophoretic manipulation of living cells and micro-organisms through consideration of several effects that are likely to appear when processing biological samples. To the best of the findings, it is the first study that uses BEM for both acoustic and hydrodynamic parts and provides simulations for non-spherical particles with acoustic and hydrodynamic interactions. It is also the first study to perform acoustophoretic separation at a device level using non-spherical particles with a numerical acoustophoretic force calculation.

For future studies, particle elastic properties can be included in the simulation scheme by modeling the particles as solid elastic domains, and the effect of the change in particle elastic properties can be investigated both in and beyond the Rayleigh limit. As an improvement to the proposed method, acoustic streaming effect can be implemented to the numerical tool since living cells would require higher acoustic energy density inside the channel, which may result in acoustic streaming. Besides, contact and clumping mechanisms would be an essential improvement, especially for manipulating high concentration samples.

REFERENCES

[1] H. Bruus, “Acoustofluidics 7: The acoustic radiation force on small particles,” *Lab on a Chip*. 2012.

[2] S. Büyükkoçak, M. B. Özer, and B. Çetin, “Numerical modeling of ultrasonic particle manipulation for microfluidic applications,” *Microfluid. Nanofluidics*, vol. 17, no. 6, pp. 1025–1037, 2014.

[3] L. V. King, “On the acoustic radiation pressure on spheres,” *Proc. R. Soc. London. Ser. A - Math. Phys. Sci.*, 1934.

[4] K. Yosioka and Y. Kawasima, “Acoustic radiation pressure on a compressible sphere,” *Acta Acust. united with Acust.*, 1955.

[5] L. P. Gor’kov, “On the forces acting on a small particle in an acoustic field within an ideal fluid,” *Dokl. Akad. Nauk SSSR*, 1962.

[6] M. Settnes and H. Bruus, “Forces acting on a small particle in an acoustical field in a viscous fluid,” *Phys. Rev. E - Stat. Nonlinear, Soft Matter Phys.*, vol. 85, no. 1, 2012.

[7] M. Antfolk, C. Magnusson, P. Augustsson, H. Lilja, and T. Laurell, “Acoustofluidic, Label-Free Separation and Simultaneous Concentration of Rare Tumor Cells from White Blood Cells,” *Anal. Chem.*, vol. 87, no. 18, pp. 9322–9328, 2015.

[8] H. Lilja, T. Laurell, K. Cushing, Y. Ceder, and E. Undvall, “Reducing WBC background in cancer cell separation products by negative acoustic contrast particle immuno-acoustophoresis,” *Anal. Chim. Acta*, vol. 1000, pp. 256–264, 2017.

[9] T. Laurell, A. Lenshof, F. Garofalo, A. Urbansky, S. Scheding, and P. Ohlsson, “Rapid and effective enrichment of mononuclear cells from blood using acoustophoresis,” *Sci. Rep.*, vol. 7, no. 1, pp. 1–9, 2017.

[10] F. Petersson, L. Åberg, A. M. Swärd-Nilsson, and T. Laurell, “Free flow acoustophoresis: Microfluidic-based mode of particle and cell separation,” *Anal. Chem.*, 2007.

[11] D. Densmore *et al.*, “Rapid prototyping and parametric optimization of plastic acoustofluidic devices for blood–bacteria separation,” *Biomed. Microdevices*, vol. 19, no. 3, 2017.

[12] P. Ohlsson *et al.*, “Integrated Acoustic Separation, Enrichment, and Microchip Polymerase Chain Reaction Detection of Bacteria from Blood for Rapid Sepsis Diagnostics,” *Anal. Chem.*, vol. 88, no. 19, pp. 9403–9411, 2016.

[13] R. Barnkob, P. Augustsson, C. Magnusson, H. Lilja, T. Laurell, and H. Bruus, “Measuring density and compressibility of white blood cells and prostate cancer cells by microchannel acoustophoresis,” *15th Int. Conf. Miniaturized Syst. Chem. Life Sci. 2011, MicroTAS 2011*, vol. 1, no. December 2014, pp. 127–129, 2011.

[14] H. Wang *et al.*, “Single-cell compressibility quantification for assessing metastatic potential of cancer cells through multi-frequency acoustophoresis,” *Microfluid. Nanofluidics*, vol. 22, no. 6, pp. 1–7, 2018.

[15] K. Petersson *et al.*, “Acoustofluidic hematocrit determination,” *Anal. Chim. Acta*, vol. 1000, pp. 199–204, 2018.

[16] P. B. Muller, R. Barnkob, M. J. H. Jensen, and H. Bruus, “A numerical study of microparticle acoustophoresis driven by acoustic radiation forces and streaming-induced drag forces,” *Lab Chip*, 2012.

[17] L. Gao, C. Wyatt Shields, L. M. Johnson, S. W. Graves, B. B. Yellen, and G. P. López, “Two-dimensional spatial manipulation of microparticles in continuous flows in acoustofluidic systems,” *Biomicrofluidics*, vol. 9, no. 1, 2015.

[18] T. Yang, V. Vitali, and P. Minzioni, “Acoustofluidic separation: impact of microfluidic system design and of sample properties,” *Microfluid. Nanofluidics*, vol. 22, no. 4, pp. 1–12, 2018.

[19] Z. Liu, Y.-J. Kim, H. Wang, and A. Han, “Effects of fluid medium flow and spatial temperature variation on acoustophoretic motion of microparticles in microfluidic channels,” *J. Acoust. Soc. Am.*, vol. 139, no. 1, pp. 332–349, 2016.

[20] J. Lei, F. Cheng, K. Li, and Z. Guo, “Numerical simulation of continuous separation of microparticles in two-stage acousto-microfluidic systems,” *Appl. Math. Model.*, 2020.

[21] M. A. Şahin, B. Çetin, and M. B. Özer, “Investigation of effect of design and operating parameters on acoustophoretic particle separation via 3D device-level simulations,” *Microfluid. Nanofluidics*, vol. 24, no. 1, pp. 1–18, 2020.

[22] T. Schwarz, G. Petit-Pierre, and J. Dual, “Rotation of non-spherical micro-particles by amplitude modulation of superimposed orthogonal ultrasonic modes,” *J. Acoust. Soc. Am.*, vol. 133, no. 3, pp. 1260–1268, 2013.

[23] T. Schwarz, P. Hahn, G. Petit-Pierre, and J. Dual, “Rotation of fibers and other non-spherical particles by the acoustic radiation torque,” *Microfluid. Nanofluidics*, vol. 18, no. 1, pp. 65–79, 2014.

[24] S. Yamahira, S. I. Hatanaka, M. Kuwabara, and S. Asai, “Orientation of fibers in liquid by ultrasonic standing waves,” *Japanese J. Appl. Physics, Part 1 Regul. Pap. Short Notes Rev. Pap.*, vol. 39, no. 6 A, pp. 3683–3687, 2000.

[25] P. Hahn, I. Leibacher, T. Baasch, and J. Dual, "Numerical simulation of acoustofluidic manipulation by radiation forces and acoustic streaming for complex particles," *Lab Chip*, vol. 15, no. 22, pp. 4302–4313, 2015.

[26] A. A. Doinikov, "Acoustic radiation interparticle forces in a compressible fluid," *J. Fluid Mech.*, vol. 444, no. October 2001, pp. 1–21, 2001.

[27] J. H. Lopes, M. Azarpeyvand, and G. T. Silva, "Acoustic interaction forces and torques acting on suspended spheres in an ideal fluid," *IEEE Trans. Ultrason. Ferroelectr. Freq. Control*, vol. 63, no. 1, pp. 186–197, 2016.

[28] G. T. Silva and H. Bruus, "Acoustic interaction forces between small particles in an ideal fluid," *Phys. Rev. E - Stat. Nonlinear, Soft Matter Phys.*, vol. 90, no. 6, pp. 1–11, 2014.

[29] M. W. H. Ley and H. Bruus, "Continuum modeling of hydrodynamic particle-particle interactions in microfluidic high-concentration suspensions," *Lab Chip*, vol. 16, no. 7, pp. 1178–1188, 2016.

[30] T. Hasegawa, "Acoustic radiation force on a sphere in a quasistationary wave field—theory," *J. Acoust. Soc. Am.*, vol. 65, no. 1, pp. 32–40, 1979.

[31] P. Glynne-Jones, P. P. Mishra, R. J. Boltryk, and M. Hill, "Efficient finite element modeling of radiation forces on elastic particles of arbitrary size and geometry," *J. Acoust. Soc. Am.*, 2013.

[32] T. Baasch, I. Leibacher, and J. Dual, "Multibody dynamics in acoustophoresis," *J. Acoust. Soc. Am.*, vol. 141, no. 3, pp. 1664–1674, 2017.

[33] T. Baasch and J. Dual, "Acoustofluidic particle dynamics: Beyond the Rayleigh limit," *J. Acoust. Soc. Am.*, vol. 143, no. 1, pp. 509–519, 2018.

[34] P. L. Marston, W. Wei, and D. B. Thiessen, "Acoustic radiation force on elliptical cylinders and spheroidal objects in low frequency standing waves," *AIP Conf. Proc.*, vol. 838, no. 2006, pp. 495–499, 2006.

[35] H. Lamb, “ XV. On the uniform motion of a sphere through a viscous fluid ,” *London, Edinburgh, Dublin Philos. Mag. J. Sci.*, 1911.

[36] F. B. Wijaya, A. R. Mohapatra, S. Sepehrirahnama, and K. M. Lim, “Coupled acoustic-shell model for experimental study of cell stiffness under acoustophoresis,” *Microfluid. Nanofluidics*, vol. 20, no. 5, pp. 1–15, 2016.

[37] F. B. Wijaya, S. Sepehrirahnama, and K. M. Lim, “Interparticle force and torque on rigid spheroidal particles in acoustophoresis,” *Wave Motion*, vol. 81, pp. 28–45, 2018.

[38] P. Hahn, J. Wang, and J. Dual, “A Parallel Boundary Element Algorithm for the Computation of the Acoustic Radiation Forces on Particles in Viscous Fluids,” no. May, pp. 2–5, 2013.

[39] M. Li, H. E. Muñoz, K. Goda, and D. Di Carlo, “Shape-based separation of microalga Euglena gracilis using inertial microfluidics,” *Sci. Rep.*, vol. 7, no. 1, pp. 1–8, 2017.

[40] J. Nam *et al.*, “Sheathless shape-based separation of candida albicans using a viscoelastic non-newtonian fluid,” *Micromachines*, vol. 10, no. 12, pp. 1–14, 2019.

[41] A. Lenshof and T. Laurell, “Acoustophoresis,” in *Encyclopedia of Nanotechnology*, 2015.

[42] G. G. Stokes, “On the effect of the Internal friction of fluids on the motion of pendulums - Section III,” *Trans. Cambridge Philos. Soc.*, 1850.

[43] R. Y. S. Lai and L. F. Mockros, “The Stokes-flow drag on prolate and oblate spheroids during axial translatory accelerations,” *J. Fluid Mech.*, 1972.

[44] S. Kirkup, “The boundary element method in acoustics: A survey,” *Applied Sciences (Switzerland)*. 2019.

[45] M. Costabel, “Principles of boundary element methods,” *Comput. Phys. Reports*, 1987.

[46] B. Çetin, M. B. Özer, E. Çağatay, and S. Büyükkoçak, “An integrated acoustic and dielectrophoretic particle manipulation in a microfluidic device for particle wash and separation fabricated by mechanical machining,” *Biomicrofluidics*, vol. 10, no. 1, 2016.

[47] B. Cetin, “Encyclopedia of Microfluidics and Nanofluidics,” *Encycl. Microfluid. Nanofluidics*, no. January, 2013.